ULTRAVIOLET ABSORBANCE AND CIRCULAR DICHROISM ANALYSIS OF DNA OLIGOMERS CONTAINING ADENINE TRACTS

by

YEE CHEE LIM

B.Sc., The University of Saskatchewan, 2004

A THESIS SUBMITTED IN PARTIAL FULFILMENT OF
THE REQUIREMENTS FOR THE DEGREE OF

MASTER OF SCIENCE

in

THE FACULTY OF GRADUATE STUDIES

(Chemistry)

THE UNIVERSITY OF BRITISH COLUMBIA

April 2007

Abstract

"A-tract" is defined as phased runs of at least four consecutive adenines, i.e. $(dA)_n \cdot (dT)_n$, where $n \geq 4$. The B*-form of DNA characteristic of A-tracts is distinct from the canonical B-DNA, with high base propeller twist and a narrower minor groove. The B* -form of DNA was examined using UV absorption and circular dichroism (CD) spectroscopy in order to estimate the extent of B*-type conformation adopted by 12-mer DNA oligomers containing different A-tract lengths. The systematic variation aims to study how the propensity towards B*-DNA formation depends on different A-tract lengths and different base compositions flanking the A-tract. CD and UV melting experiments indicate that B*-form has distinctive spectral signatures. The structural formation of B*-DNA increases with A-tract length, but can be affected by the location of the A-tract within the sequence as well as neighboring AA/TT, AT, and TA base pairs.

The spectroscopic results generally correlate well with differential scanning calorimetry (DSC) data. The calorimetrically obtained results were compared with thermodynamic parameters predicted by the Santa Lucia nearest-neighbor (NN) model. Disagreements between experimental and predicted thermodynamic values exist particularly for mixed AT sequences and those with the same number of NN parameters. Such discrepancies may be caused by different stabilities resulting from various extent of B*-type formation within a given DNA sequence. Since NN estimates of the melting temperature do not adequately account for structural differences, the incorporation of additional structural information may have a pronounced impact on thermodynamic variables and will help to improve the NN model considerably. Consequently, this allows for a more accurate prediction of the stability of short DNA sequences (< 25 base

pairs), often used in molecular biology applications involving sequence dependent hybridization reactions. In light of the increasing interest in the development of locked nucleic acids (LNA) for probe and primer design and theurapeutic applications, the thermodynamics and spectroscopic studies on the structural effects of the incorporation of LNA nucleotides on the A-tract structure will also be presented.

Table of Contents

List of Tables

List of Figures

List of Abbreviations

A	Adenine
bp	Base pairs
C	Cytosine
CD	Circular Dichroism
DNA	Deoxyribonucleic Acid
DSC	Differential Scanning Calorimetry
EDTA	Ethylenediaminetetraacetic Acid
G	Guanine
LNA	Locked Nucleic Acid
NN	Nearest-neighbor
PCR	Polymerase Chain Reaction
PNA	Peptide Nucleic Acid
RNA	Ribonucleic Acid
SNP	Single Polynucleotide Polymorphism
T	Thymine
T_m	Melting temperature
TDS	Thermal Difference Spectra
UV	Ultraviolet

Acknowledgments

Thanks are due to helpful guidance from my supervisors, Michael Blades and Robin Turner. I sincerely thank Georg Schulze, Curtis Hughesman, Fred Rossell for their extensive discussions and critical comments, and Marcia Yu for her involvement in the final stages of thesis.

Special thanks to my brother, Yee Cheng Lim, who has always been a source of motivation.

Finally, my heartfelt gratitude goes to Jeffrey Robert Johnston, for his feedback and continuous encouragement throughout the course of this study.

Chapter 1

Introduction

Most of the work presented in this thesis is directed toward better understanding the sequence-dependent determinants of secondary structure of DNA (and certain non-natural) oligonucleotides and concomitant effects on the stability of the duplex form. In this introductory chapter, the well-known right-handed anti-parallel double helical structure of B-DNA will be addressed. Other DNA conformations such as A-DNA and Z-DNA will also be discussed to exemplify other variant forms of DNA, which is largely attributed to the sequence-dependent nature of DNA structure. The unique structure of B*-DNA is of considerable interest because its relationship with the presence of adenine tracts (A-tracts) represents a good example of sequence specific conformational modulations. Structural studies of A-tracts form the basis for understanding DNA curvature and deformation, which has significant relevance in terms of sequence specific regulation of genetic issues at the molecular level.

1.1 Canonical Conformations of DNA

The foundation of modern molecular biology starts with the discovery of the classic deoxyribonucleic acid (DNA) duplex structure, initially described in 1953 by Watson and Crick[1, 2]. There are many excellent reviews, giving detailed descriptions of the structure of DNA[3-10]. Therefore, only a brief summary of the DNA structure will be provided here to facilitate discussion within the context of this thesis.

DNA consists of two anti-parallel polynucleotide strands, one in the 5' to 3' direction and the other in the 3' to 5' direction. The nucleotide building blocks consist of a sugar moiety (deoxyribose), a phosphate linker, and a nucleobase. Four different nucleotide bases occur in DNA: adenine (A), thymine (T), guanine (G), and cytosine (C). Each base within a rung of the DNA ladder is always paired with its complementary base, such that A always pairs with T through two hydrogen bonds, and G always pairs with cytosine (C) through three hydrogen bonds. According to Chargaff's rules, the complementary base pairing results in equal numbers of A and T, and equal numbers of G and C in a DNA molecule[4]. The intertwined strands make two grooves of different widths, referred to as the major groove and the minor groove, which may facilitate binding with specific drugs. For example, the polyamide antibiotics netropsin[5] and distamycin[6] bind into the minor groove of DNA by recognizing AT-rich sequences.

In the investigation of DNA secondary structures, early diffraction studies led to the identification of two distinct conformations of the DNA double helix, depending on factors such as base compositions and environmental conditions (i.e. relative humidity and salt concentration). The structural features of the three most common conformations of DNA, A-, B-, and Z-DNA, is shown in Figure 1.1. At high humidity (92%) and low salt, the dominant structure is called B-DNA[7-9] and at low humidity (75%) and high salt, the favoured form is A-DNA[10-12]. In 1979, a left handed helix formed by a synthetic hexamer d(CGCGCG) was discovered and is now known as Z-DNA[13].

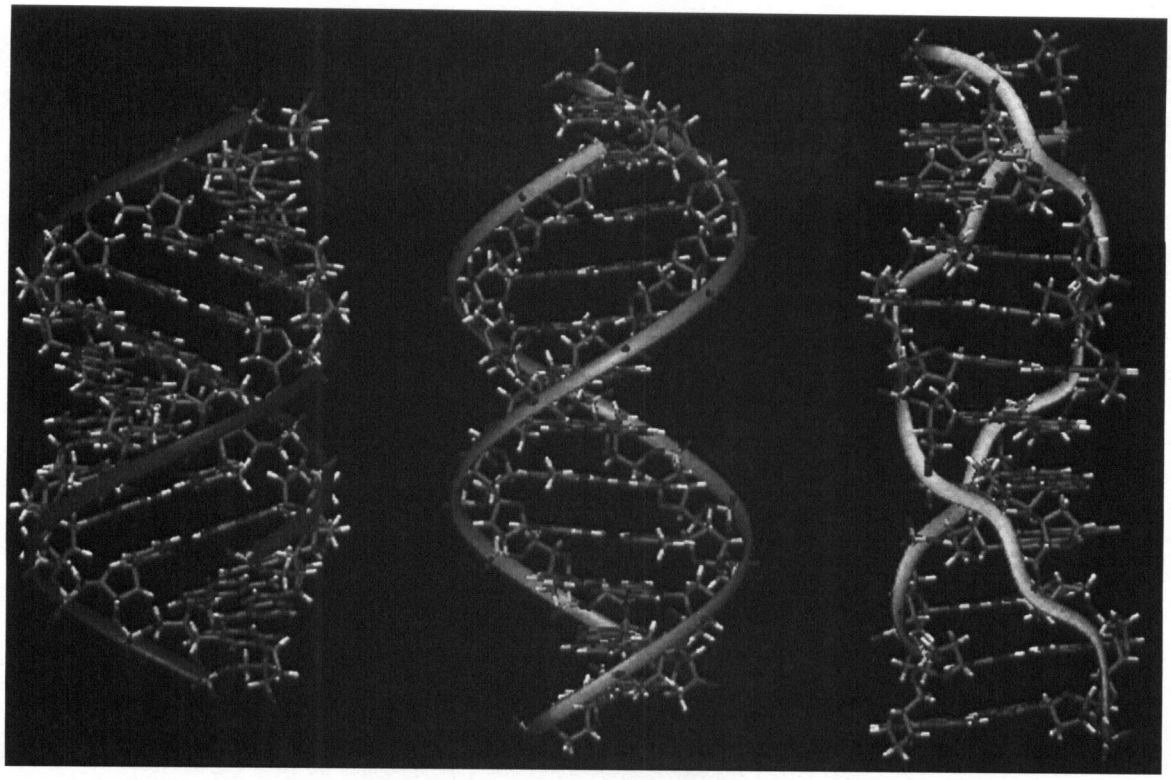

Figure 1.1: The side projections of the crystal structures of A-, B-, and Z-DNA (shown from left to right). A- and B-DNA are right-handed helices, whereas Z-DNA is a left handed double helix with a backbone that follows a zig-zag pattern. Adapted from http://upload.wikimedia.org/wikipedia/en/b/b9/A-B-Z-DNA_Side_View.png

The morphological difference found in DNA originates from the variations in the preferred sugar conformations of the deoxyriboses and the orientation of the base relative to the sugar. The deoxyribose in DNA, where the stabilizing 2'-hydroxyl effects are absent, exists in fast equilibrium between C2'- *endo* and C3'- *endo* conformations, which are shown in Figure 1.2, with a relatively low energy barrier[14] (~2 kcal mol^{-1}). For deoxyribose, the C2'- *endo* conformation is slightly lower in energy (0.5 – 1.0 kcal mol^{-1})[14] compared to the C3'- *endo* and this explains why the C2'- *endo* sugar conformation of DNA is preferred. In most double-helical nucleic acids, except Z-DNA, the rotation of a base around its glycosidic bond is in the *anti* conformation[4].

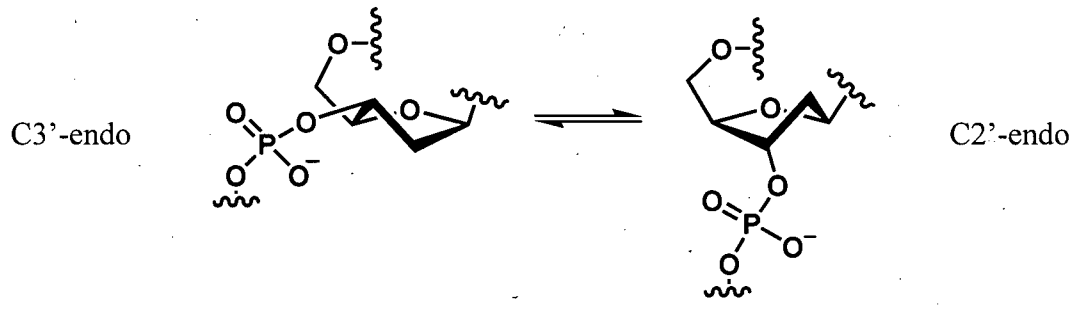

Figure 1.2: The C2'-endo and C3'-endo sugar conformations of DNA. The preferred geometry of intrinsic sugar puckering and the decreased phosphate-phosphate repulsion in C2'-endo conformation results in it being a lower energy structure compared to C3'-endo.

1.1.1 B-DNA

Natural double-stranded DNA exists at physiological pH as a B-DNA (B-form) helix. The C2'- *endo* sugar conformation gives rise to the B-form helix[4]. The conformation of B-DNA is defined by a helical repeat of 10.6 base pairs per turn[15, 16], a narrow minor groove, and a widened major groove. In B-DNA, the major and minor grooves are of equal depth since the bases sit directly on the axis[17]. The B-form is favored by AT-rich DNA, indicative of the role of sequence in determining conformational stability.

1.1.2 A-DNA

The sugar pucker in A-DNA adopts the C3'-*endo* conformation[4]. In comparison to B-DNA, the helical structure of A-DNA is more uniform, characterized by a deeper major groove, and a narrower minor groove[17]. Besides a helical repeat of 11 base pairs per turn[3, 4], the most distinguishing feature of A-DNA relates to the displacement of these base pairs at a tilt of 20° with respect to the helix axis[3, 4, 17]. A-DNA is less flexible than B-DNA and the rigidity is proposed to have biological significance. For example, DNA

replication can occur at a higher degree of fidelity in the A-form due to the added stiffness[5]. Sequences containing G-tracts, which are defined by sequences with homo-GC in base composition and particularly rich in GG base steps (or CC base steps) such as poly(dG)·poly(dC), tend to adopt the A-form[18]. At low relative humidity, B-DNA undergoes a reversible conformational change to A-DNA. The B to A conformational change plays an important role in gene regulatory processes of DNA polymerase and HIV-1 reverse transcriptase, both of which are found in an A-like structure[19].

1.1.3 Z-DNA

Under high salt conditions, the alternating copolymer poly[d(C-G)] was observed by Wang *et al.*[20] to adopt a conformation unexpectedly different from A- or B-DNA, called Z-DNA. Aside from its left-handed helical sense, Z-DNA has 12 base pairs per helical turn. The base pairs are displaced in the opposite direction from those in A-DNA, resulting in a deep minor groove and a flat major groove[4, 17]. The overall chain sense in Z-DNA is directed downward at the left of the minor groove and upward at the right, as opposed to the right-handed family of DNA duplexes. The sugar and glycosidic bond alternate in the following manner[4]: C2'- *endo* in *anti* dC or dT and C3'- *endo* in *syn* dG or dA. For Z-DNA, the requirement of purine/pyrimidine alternation is due to the preference of the *syn* conformation[21, 22]. Some examples of sequences known to adopt the Z-form include poly (dG-dC)·poly(dG-dC) and poly(dG-dT)·poly(dA-dC), with exception of poly(dA-dT)·poly(dA-dT). The preference of alternating G and C over A and T does not yet have a clear explanation[17].

1.2 Non-canonical conformation of DNA

1.2.1 B*-DNA

The formation of various structural forms of DNA, discussed up to this point, depend on factors such as salt, hydration, and base pair composition. As more highly resolved methods for structural studies have become available, it has been found that some B-DNA sub-conformations also exist. Analysis of poly(dA)·poly(dT) helices have been observed to pack in the crystal lattice differently from ordinary B-DNA[23]. This homopolymeric DNA duplex displays 10.1 ± 0.1 base pairs per turn[24], setting it apart from the common B-DNA structure with alternating or random distributions of bases[25]. The minor groove is considerably narrower in poly(dA)·poly(dT) than in standard B-form DNA. Other unusual properties of poly(dA)·poly(dT) include resistance to transformation into other helical forms[23], unlike the standard B-DNA, under different conditions of relative humidity and salt concentration[24]. If the salt concentration of the environment is raised (or the relative humidity lowered), the normal B → A transition does not occur. Instead, a disproportionation of the double helix into a triple helix and a single polynucleotide chain is observed, similar to the poly(A)·poly(U) system[25]. Despite these differences, the structure of poly(dA)·poly(dT) differs only slightly from that of the canonical B-DNA, and thus, its conformation is referred to as B*-DNA.

The unusual structure of poly(dA)·poly(dT) is stabilized by purine-purine base stacking interactions and by additional hydrogen bonds, both of which arise from the high propeller twist of the base pairs. The propeller twist feature refers to the rotation of the bases along their longitudinal axis[24]. The local, sequence-dependent distortions of structure are primarily associated with changes in the orientation of bases in order to

maximize base stacking interactions. An energetically favorable hydration reaction in the minor groove is thought to stabilize the B*-form of the polynucleotide[26, 27].

1.2.2 Relationship between B*-form and A-tracts

The helical irregularities found in the crystal structure of the *Eco RI* recognition site containing the dodecamer sequence, d(CGCGAATTCGCG), led to the realization that DNA secondary structure is indeed sequence-dependent[28, 29]. The next important study of sequence effects came from the investigation of the intrinsically curved or bent kinetoplast DNA[30], in which regions of curvature were found to result from the presence of properly phased stretches of adenine, known as A-tract[30, 31] ($dA_n \cdot dT_n$), within the helical repeat. Since then, additional experimental evidence has been accumulated to understand the behavior of A-tracts. The fundamental aspect of the A-tract requires that at least four[32 – 35] adenine residues in tandem be present in a given oligonucleotide sequence, with only AA (equivalently TT) or AT base-steps, and no TA base-steps[18]. Molecular dynamics studies further identified the formation of sequence dependent hydration patterns in the minor groove, often called "spine of hydration", near the A-rich region[36]. The spine of hydration is often suggested to play a critical role in the stabilization of the B*-form of DNA in solution[37, 38]. In addition, the high propeller twist of the AT base pairs found in the more rigid and less flexible B*-form structure differentiates it from the common B-form, thus maximizing purine-purine stacking interactions[32, 33].

Curved fragments of oligonucleotides containing A-tracts have been detected from its retarded movement during electrophoresis in polyacrylamide gels[39 – 41] because curved structures are hindered more than straight molecules when migrating through the

gel pores[41]. The necessity for a continuous run of adenines in order to observe strong bending anomalies is supported by experimental evidence that the disruption of the run of A's within an A-tract by a G, C, or T base produces a near normal gel migration pattern of the respective substituted concatamers[42]. The electrophoretic mobility of phased A-tracts is not drastically affected by the sequence within the GC containing regions connecting adjacent A-tracts[43]. Other properties of the A-tract include the progressive narrowing of the minor groove toward the 3' end[44–47] and the existence of bifurcated hydrogen bonds[24, 37]. It should be noted that bifurcated hydrogen bonds are a consequence of the high propeller twisting in A-tracts, rather than being the driving force for the formation of A-tracts. Replacing AAA with the inosine (I) mutant AIA, which does not form bifurcated hydrogen bonds resulted in little change in anomalous gel retardation[48], suggesting that conformational stability due to bifurcated hydrogen bonds may be slight, if any[37].

1.2.3 Origin and Stabilization of B*-form

Several theoretical models have been developed to understand the sequence-dependent effects of A-tracts on conformational stability of DNA and to relate it to DNA bending.

The junction model proposes that the A-tract region exists in a non B-DNA form with base pairs at a negative inclination relative to the overall helix axis[49, 50]. Parallel stacking of the highly inclined base pairs in an A tract causes the non-A-tract DNA helix axis to form an angle with the A-tract DNA helix axis. A deformation of the helix axis is then observed at the junctions between A-tracts and B-DNA[46].

The wedge model[51, 52] attributes the non-parallel stacking of adjacent base pairs to deflections in every AA dinucleotide step[35]. Each non-parallel AA step effectively forms a wedge that can curve the helix axis if they occur within the DNA helical repeat.

More recently, it has been proposed that A-tracts stabilize the B*-form through cations localized in the A-tract minor groove more dominantly than the A-tract major groove[21]. The localization of cations depends on electrostatic interactions with the functional groups of the DNA bases and backbone. Preferential localization of cations within the minor groove of A-tracts can cause asymmetric distribution of phosphate neutralization, which in turn can cause narrowing of the minor groove and bending of the helical axis.

1.2.4 Biological Impact of A-tract DNA Oligomers

The biological relevance of A-tract structures is linked to its distinctive structural properties. A-tracts serve important roles in several biological processes, including DNA replication and packaging, chromosome segregation, and transcriptional regulation[24]. For example, A-tracts have been found to act as upstream promoters that activate transcription in yeast[53]. Another example involves that of histone H1 which preferentially binds and aggregates scaffold-associated regions via the numerous A-tracts present within these sequences in order to regulate transcriptional processes[54]. In terms of biological recognition, the sequence-specific deformations caused by A-tracts have been found to be involved in activities of regulatory proteins. For example, the mechanism by which the *Bacillus subtilis* LrpC protein interacts with DNA depends on the curved characteristics of sequences containing phased A-tracts[55].

1.3 Spectroscopic Characterization of A-tract DNA Oligomers

1.3.1.1 UV-Visible Absorption Spectroscopy

UV-Visible absorption spectroscopy is based on the absorption of light due to the interaction of the oscillating electromagnetic field of the radiation with the electrons in the molecule. If the frequency of electromagnetic field corresponds to the energy difference between the ground and excited states, the electrons in the molecule are shifted to higher energy levels. This increase is equal to the energy E of the photon, which is related to the frequency υ and the wavelength λ of the radiation by the following equation:

$$E = h\upsilon = hc / \lambda \qquad (1.1)$$

where h is the Planck's constant and c is the velocity of light. The change in energy may be in the electronic, vibrational, or rotational energy of the molecule. During the UV light absorption process, the energy differences correspond to those of the electronic states of atoms and molecules and causes transitions of electrons from the ground state to an excited state[56]. The absorption process is extremely fast, occurring in about 10^{-15} seconds[57]. An illustration of the absorption process is shown schematically in Figure 1.3.

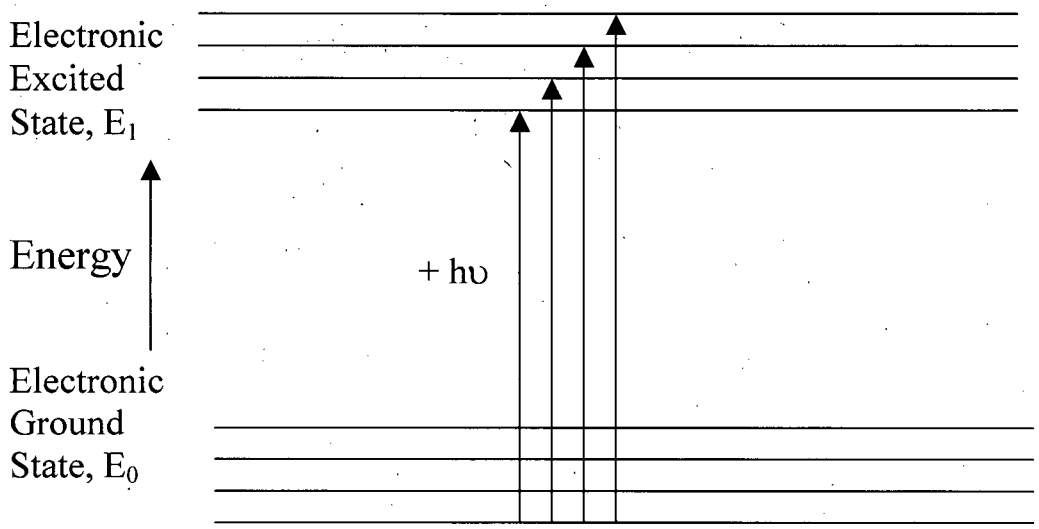

Figure 1.3: Schematic energy level diagram for the UV absorption process. Two electronic levels are shown, together with the corresponding vibrational sublevels which are represented by the horizontal lines. The arrows represent the transition of electrons from the ground state to the various vibrational levels of the first excited state upon absorption of UV photons.

The amount of light absorbed by the sample is described by the Beer-Lambert law, which is the relationship between the light intensity entering the absorbing medium, I_o, and the light intensity leaving the absorbing medium, I:

$$\log (I_o / I) = A = \varepsilon C l \qquad (1.2)$$

where A is the absorbance, ε is the molar absorption coefficient, C is the concentration of the sample, and l is the sample pathlength. ε has the units L mol^{-1} cm^{-1} and is characteristic of the molecule of interest.

Apparent deviations from the Beer-Lambert law may arise from instrumental and sample artifacts such as light scattering, a non-monochromatic light source, inhomogeneous sample, non-linear photodetector, and absorption by the cuvette[56, 57].

Molecular properties of the sample, such as sample aggregation or complex formation as the concentration is changed, may also cause deviations from linearity[56, 57].

The fundamental basis for the UV absorption bands of nucleic acids is correlated with the types of bonds they contain. Electrons forming single bonds are called σ electrons[56]. The characteristic functions and charge densities of σ electrons are rotationally symmetrical with respect to the bond axis[56]. Electrons responsible for double bonds are called π electrons, the characteristic functions and charge densities of which have a nodal plane through the bond axis[56]. In unsaturated systems, π electrons predominantly determine the energy levels of the electrons, which are excited by the absorption of ultraviolet light. *n* electrons refer to the unshared electrons or non-bonded electrons in molecules containing atoms like nitrogen and oxygen. In bonding systems, σ electrons are more strongly bound than the π electrons while in the antibonding levels, the σ* level has higher energy compared to the π* level[56]. Possible electronic transitions involving σ, π, and *n* electrons are shown in Figure 1.4.

Based on the properties of the conjugated ring systems of nucleic acid bases, conformational changes in DNA can be followed by observing the shifts in their UV absorption spectra. The presence of chromophores in DNA molecules can be identified by examining the wavelength corresponding to the absorption maximum, λ_{max}. λ_{max} is affected by the type of chromophore present as a result of the difference in the electronegativities of the elements forming the multiple bonds[56]. UV absorption by a single C=C double bond exhibits an absorption maximum at ~ 180 nm[56]. When the conjugation of double bonds increases, the energies of the molecular orbitals lie closer together and the UV peaks associated with the $\pi \rightarrow \pi^*$ transition are shifted towards

longer wavelengths. In general, the absorption bands of nucleic acid bases normally found in the near UV and visible regions arise from either $\pi \rightarrow \pi^*$ or $n \rightarrow \pi^*$ transitions[58]. The allowed $\pi \rightarrow \pi^*$ transitions at 260 nm are a lot more intense than the $n \rightarrow \pi^*$ transitions which are symmetry forbidden and consequently of weak intensity.

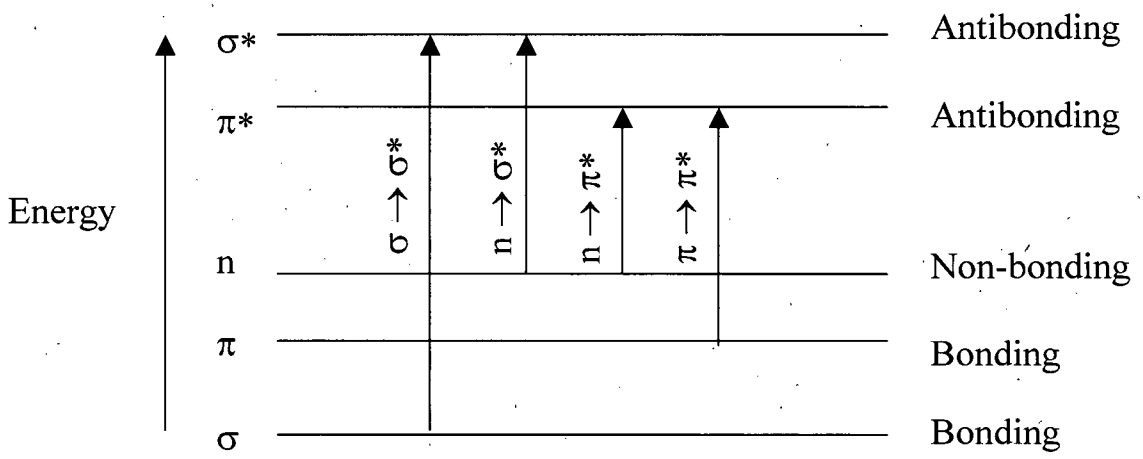

Figure 1.4: An illustration of the energies for the various types of molecular orbitals. The arrows depict the four possible types of electronic transitions ($\sigma \rightarrow \sigma^*$, $n \rightarrow \sigma^*$, $n \rightarrow \pi^*$, and $\pi \rightarrow \pi^*$) among different molecular energy levels brought about by the absorption of radiation. *(Reprinted with permission from Skoog, D. A., Holler, F. J., and Nieman, T. A. Principles of Instrumental Analysis, 5th edition, p. 331. Copyright 1998 by Harcourt Brace & Company)*

1.3.1.2 UV Absorbance Spectra of Nucleic Acids

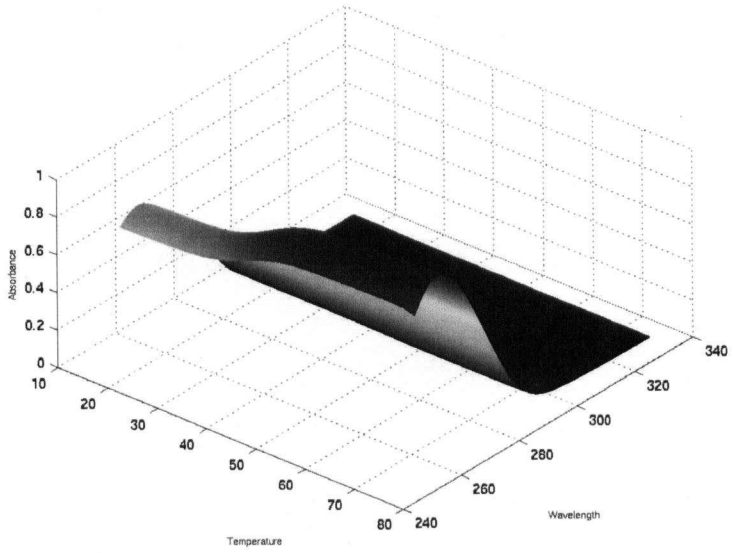

Figure 1.5: UV absorbance surface as a function of temperature and wavelength of the homopolymer $d(A)_{12}$ (EE07). See Table 2.1 on page 21 for a complete list of other sequences used in this study.

The ease of measurement, simplicity of the instrumentation, and requirement for low concentrations (~ 5 μg/ml)[59] of DNA oligonucleotide samples have made UV absorbance spectroscopy a common method for studying DNA transition thermodynamics. DNA duplex melting and formation can be easily monitored through changes in UV absorbance. The 3-dimensional melting surface of $d(A)_{12}$ (EE07) shown in Figure 1.5 has a peak maximum positioned at 259 nm. Certain of the subunits of nucleic acids (purines) have an absorbance maximum slightly below 260 nm while others (pyrimidines) have a maximum slightly above 260 nm[58]. Therefore, the UV absorbance maxima of DNA polymers can vary somewhat depending on their sequence composition.

When a solution of duplex DNA is heated, the base pairs are separated as the hydrogen bonds between them are broken. This results in the formation of single-stranded DNA and this process is commonly referred to as "DNA denaturation" or "melting". The qualitative changes accompanying the denaturation process can be followed by monitoring the difference in UV absorbance between the two states at a single wavelength (usually 260 nm) as the temperature increases. DNA denaturation is a reversible process upon slow cooling conditions to below its T_m.

The stability of the double helix is not only determined by the hydrogen bonds between paired bases but also by the stacking of parallel planes of the bases[60]. Base-stacking is due to the overlapping of the π-electron orbitals of the planar bases. Because of this π-electron interaction, double-stranded DNA exhibits a lower light absorbance at 260 nm than single-stranded DNA[61]. This hypochromicity effect, which occurs as a consequence of the disruption of the electronic interactions among neighboring bases, is often used to understand nearest-neighbor base pair interactions[62].

For short DNA oligomers, the UV absorbance values at 260 nm monitored over a range of temperatures results in a sigmoidal-shaped "melting curve". The temperature at which 50% of the DNA is denatured is called the melting temperature, denoted as T_m. The stability of the DNA duplex, and hence its T_m, depends on several factors, including buffer composition (salt concentration and identities of the ions in solution), base composition (regions with alternating pyrimidine/purine steps and AT regions melt more readily than GC regions; T_m increases with G·C content), the length of the DNA sequence (shorter lengths of DNA will have lower T_m), and the secondary structure of the DNA[62]. Due to the various factors that can affect T_m, it is difficult to predict accurately the exact

melting temperature of a given sequence. The practical importance of having a good estimate for T_m is exemplified in the determination of appropriate PCR primer annealing temperatures. Temperatures too far beyond T_m will produce insufficient primer-template hybridization resulting in low PCR product yield. Temperatures significantly lower than T_m may possibly lead to non-specific products caused by a high number of base pair mismatches. In addition, information about the T_m can be used to determine the minimum length of an oligonucleotide probe needed to form a stable double helix with a target gene at a particular temperature[63].

1.3.1.3 Two-State Model of DNA Denaturation

To probe the melting process of DNA oligonucleotides, an important assumption is that the melting process is a reversible transition between double-stranded and single-stranded DNA and is commonly referred to as the "two-state process"[64, 65]. In this model, each DNA molecule is considered to be either totally in the double helix form or totally dissociated. The melting temperature, T_m, defined as the temperature at which half of the nucleic acids are in the single-strand form, can be extracted from the experimental data. The two-state model is usually regarded as valid for short ($\leq$12 bp) oligonucleotides[66].

1.3.2 Circular Dichroism

1.3.2.1 Theoretical Background of Circular Dichroism

Circularly polarized light is produced from two linearly polarized and mutually perpendicular beams of equal maximum magnitude that are out of phase by $\pi/2$. Circular dichroism (CD) is the difference in absorption for left and right circularly polarized light by the same transitions observed in normal absorption spectroscopy[67]. Therefore, Beer's law will be obeyed for either rotation of circularly polarized light, and the difference in absorption, ΔA, is given by:

$$\Delta A = A_L - A_R = (\varepsilon_L - \varepsilon_R)\, lC = \Delta\varepsilon lC \qquad (1.3)$$

where l is the pathlength, C is the molar concentration, and the subscripts L and R denote the left and right rotation of the light, respectively. $\Delta\varepsilon$ is characteristic of the molecule being examined and depends on the wavelength of light. The CD bands may be either positive or negative, depending on which rotation of light is absorbed more strongly. According to equation 1.3, CD can arise only in the spectral region where the sample absorbs light. There cannot be a measurable difference if the absorbance is close to zero.

An optically active molecule will absorb the left circularly polarized light differently from right circularly polarized light. Consequently, the transmitted light appears as elliptically polarized light. Thus, the ellipticity, θ, usually measured in units of millidegrees (mdeg), is defined by the ratio between the minor axis and the major axis of the elliptically polarized right[68]:

$$tan\theta = \frac{(E_R - E_L)}{(E_R + E_L)} \qquad (1.4)$$

where E_R and E_L are the magnitudes of the electric field vectors of the right-circularly and left-circularly polarized light, respectively. When E_R equals E_L (when the absorbance of right- and left-circular polarized light are the same), θ is 0° and the light remains linearly polarized. When either E_R or E_L is equal to zero (when the circular polarized light in completely absorbed in only one direction), θ is 45° and the light emerges as circularly polarized[68]. Since the intensity of light, I, is proportional to the square of the electric-field vector, the ellipticity becomes:

$$\theta(radians) = \frac{(I_R^{1/2} - I_L^{1/2})}{(I_R^{1/2} + I_L^{1/2})} \tag{1.5}$$

The natural logarithm form of equation (1.2) is:

$$I = I_0 e^{-A ln 10} \tag{1.6}$$

By substituting equation (1.5) into (1.6), ellipticity can be rewritten as:

$$\theta(radians) = \frac{(e^{\frac{-A_R}{2} ln 10} - e^{\frac{-A_L}{2} ln 10})}{(e^{\frac{-A_R}{2} ln 10} + e^{\frac{-A_L}{2} ln 10})} = \frac{e^{\Delta A \frac{ln 10}{2}} - 1}{e^{\Delta A \frac{ln 10}{2}} + 1} \tag{1.7}$$

Equation (1.7) can be simplified using a first-order Taylor series approximation. Since $\Delta A << 1$, terms of ΔA can be discarded in comparison with unity. Converting from radians to degrees yields:

$$\theta(degrees) = \Delta A(\frac{ln 10}{4})(\frac{180}{\pi}) \tag{1.8}$$

The linear dependence of solute concentration and pathlength is removed by defining molar ellipticity as:

$$[\theta] = \frac{100\theta}{Cl} \tag{1.9}$$

Then combining the last two expressions with Beer's Law, molar ellipticity becomes:

$$[\theta] = 100\Delta\epsilon(\frac{ln10}{4})(\frac{180}{\pi}) = 3298\Delta\epsilon \tag{1.10}$$

Therefore, the relationship between CD and normal absorption spectroscopy is embedded in equation (1.10). Since CD monitors transitions only at their wavelength of maximum absorption, CD shapes are simpler, and the spectra are easier to interpret.

1.4 Importance and Applications of DNA Thermodynamics

The stability of duplex DNA strongly depends on temperature and solution conditions, particularly for short oligonucleotides. Therefore, thermodynamic profiles of DNA are of fundamental and practical importance in understanding and predicting the sequence-dependent secondary structures of nucleic acids.

The application of thermodynamic parameters for nucleic acids are found in many molecular biology applications such as the design of hybridization probes using natural or modified nucleic acid bases for DNA microarrays or PCR, which are used in a variety of genotyping and other genomic applications (e.g. gene expression profiling, hereditary disease diagnostics, etc). Successful probe and primer design for such applications relies heavily on the ability to predict the thermodynamic stability of the complexes formed by the oligonucleotide probes. The choice of optimal conditions for hybridization experiments, minimum length of a probe required for hybridization, and probe and primer

stability, are heavily dependent on accurate thermodynamic predictions[69-71]. For example, the melting temperature (T_m) of different probes in DNA microarray registers must be accurately estimated using an appropriate nearest-neighbor thermodynamic model that permits the iterative selection of a set of probes with a minimal T_m variability[72]. In multiplex PCR, where all the amplifications must occur under the same conditions, inaccurate T_m predictions lead to poor design of an optimal sequence and consequently, the amplification or detection of wrong sequences[73-76].

Modified, non-naturally occuring nucleic acids such as peptide nucleic acids (PNA)[77, 78] and locked nucleic acids (LNA)[79, 80] are useful for their enhanced hybridization affinities towards single-stranded DNA or RNA. For example, they have been used for their ability to distinguish between ssDNA and ssRNA in the development of non-labeled oligonucleotide probes[81] and antisense technologies[82, 83]. Substitution of one or more DNA nucleotides with a locked nucleotide in oligonucleotide probes (LNA) has shown to significantly increase the thermal stability of the LNA:DNA duplex, and to improve the discrimination between perfectly matched and mismatched target nucleic acids. These two features are exploited for enhancing hybridization efficiencies under any prescribed conditions.

1.5 Differential Scanning Calorimetry

Calorimetric measurements allow for the evaluation of thermodynamic properties of a system, which is required to understand the relationship between energy changes involved in a chemical or physical-chemical process[84].

Differential scanning calorimetry (DSC) is a type of calorimetric technique that measures the heat capacity, C_p, of a system as it varies with temperature[73]. By heating or cooling a sample and reference material (which consists of a sealed empty aluminium pan) under the condition that they are always maintained at the same temperature, it is possible to measure the changes in C_p that accompany heat-induced structural transitions in the sample[73]. DSC measurement is often used to determine the thermal stability and reversibility of DNA denaturation process. One advantage of DSC is that a direct measurement of thermodynamic parameters of nucleic acids can be obtained. However, compared to spectroscopic methods (typically UV measurements), a relatively larger amount of sample is required for DSC experiments[85].

In a typical DSC experiment, the excess heat capacity curve of the DNA solution relative to the reference buffer, C_p^{ex}, is recorded as a function of temperature for the thermally induced transition of an oligomeric DNA sample[86]. Valuable thermodynamic information, such as the difference in heat capacity (ΔC_p), enthalpy (ΔH°), and entropy (ΔS°), can be obtained from a single DSC curve. Integration of C_p^{ex} with respect to temperature, as shown in equation (1.11), yields ΔH°.

$$\Delta H^\circ = \int C_p^{ex}\, dT \qquad (1.11)$$

The difference between the initial and final baselines of the DSC profile gives a direct measure of the heat capacity change, ΔC_p, accompanying the transition[73]. By

converting the experimental ΔC_p^{ex} *versus* T curve to a $\Delta C_p^{ex}/T$ *versus* T curve yields the value of ΔS° using equation (1.12):

$$\Delta S^\circ = \int (C_p^{ex}/T)\, dT \qquad (1.12)$$

Based on equation (1.13), the corresponding value of free energy change, ΔG°, can also be determined at any temperature.

$$\Delta G^\circ = \Delta H^\circ - T\Delta S^\circ \qquad (1.13)$$

where T is in Kelvin, ΔH° is in cal mol^{-1}, and ΔS° is in units of cal K^{-1} mol^{-1}. Equation (1.13) assumes that ΔC_p is zero, which means that ΔH° and ΔS° are assumed to be temperature independent. This approximation is commonly used for analyzing the hybridization thermodynamics of nucleic acids[85].

The slope and intercept from a $1/T_m$ *versus* ln C_T plot has been shown to be equal to $R(n\text{-}1)\,\Delta H^\circ_{V.H.}$ and $[\Delta S^\circ_{V.H.} - (n\text{-}1)R\ln 2 + R\ln n]\Delta H^\circ_{V.H.}$, respectively[86]. Here, n represents the molecularity of the complex (the number of strands that associate), R is the gas constant, $\Delta H^\circ_{V.H.}$ is the van't Hoff enthalpy, $\Delta S^\circ_{V.H.}$ is the van't Hoff entropy, and C_T is the total strand concentration. Comparison between $\Delta H^\circ_{V.H.}$(model-dependent) and ΔH° (model-independent) allows one to evaluate if the two-state model holds for a given DNA melting transition, but often results in large discrepancies[87-92]. If ΔH° *cf.* $\Delta H^\circ_{V.H.}$ reveals that the two-state model does not hold, then one explanation would be that a non-two-state transition[93] is involved. Another interpretation is related to the differences in hydration between the duplex-stranded groups and single-stranded groups giving rise to an increase in the heat capacity[89, 92, 94]. The thermodynamic analysis of the oligonucleotides used in this study assumes a two-state approximation and a negligible change in heat capacity at constant pressure, ΔC_p. A change in heat capacity is generally

regarded as a dominant factor accounting for a difference between the van't Hoff enthalpy and the calorimetric enthalpy that can significantly affect the thermodynamic properties of duplex formation[95].

1.6 Concept of the Unified Nearest-Neighbor Model

The first nearest-neighbor (NN) type model was initially used to predict the stability and predict the temperature-dependent behaviour of RNA[96] and was later extended to apply to DNA duplex stability[97]. The basic concept of the NN model for nucleic acids describes how the thermodynamic stability of a given sequence is dependent on the identity and orientation of neighboring base pairs[97, 98]. The nearest-neighbor approximation assumes that the stability of a DNA duplex depends on the sum of neighboring base pair interactions that accounts for hydrogen bonds in a base pair and stacking interaction between nearest-neighbor bases. Thus, the prediction of thermodynamic parameters is possible if the primary sequence is known[97]. The ten Watson-Crick DNA nearest-neighbor pair-wise combinations[97, 99] that are present in anti-parallel duplex DNA are: AA/TT; AT/TA; TA/AT; CA/GT; GT/CA; CT/GA; GA/CT; CG/GC; GC/CG; GG/CC. Here, the nearest-neighbor sequences are represented with a slash, /, separating the strands in antiparallel orientation. For example, AT/TA means 5'-AT-3' is paired with 3'-TA-5'.

The "unified" oligonucleotide NN model takes into account thermodynamic information from six research groups, with the aim to overcome the confusion arising for reasons such as differences in salt dependencies, data analysis and experimental approach[99]. These parameters were derived from multiple linear regressions of 108 sequences and solving for 12 unknowns: the ten Watson-Crick DNA NN interaction

parameters, one initiation parameter, and one correction for terminal AT pairs[99, 100]. The reliability of the unified parameters for predicting a dataset of 264 sequences ranging in length from 4 to 16 bp has been tested[100], yielding an average deviation between experimental and predicted T_m of 1.6°C. Although the unified NN model provides reasonably good thermodynamic predictions for most applications of nucleic acids[100], there have been suggestions that the possible influence of non-adjacent base pairs should also be taken into consideration. However, no other model has yet been proposed and verified, hence, the unified NN model remains the best available and is widely used.

Limitations of the unified NN model are reflected in its inadequacy to properly predict more complex sequence-dependent interactions involving DNA curvature[101-103], fraying end effects[104], triplet repeats[105], mismatches[106], hairpin structures[107], chemically modified oligonucleotides[108], and DNA dumbbells[109]. In addition, a more refined predictive model for non-canonical B-form DNA, as well as other DNA deformations associated with A-tracts, will be required to address the full dimensionality of DNA secondary structure and conformation.

1.7 Objectives

The rapid growth in nucleic acids research is attributed to the wealth of sequence information generated by the human genome project and the recent advances in both theoretical and experimental methods used. The results from a variety of studies have indicated that a combination of structural and thermodynamic data will be needed to fully understand the sequence-dependent structure of A-tract oligonucleotides for potential theurapeutic applications, given its role in several key biological processes.

Thermodynamic variables obtained by DSC measurements have shown that discrepancies exist in thermodynamic characterizations of DNA containing A-tracts. Proper explanations are needed in order to advance the basic understanding of sequence-dependent structural phenomena and to assess the degree to which local DNA distortions may contribute to the forces that drive biologically significant events. Toward this end, the major goal of this thesis is to qualitatively determine the extent to which B*-form is influenced by the presence of A-tracts through temperature-dependent UV and CD methods. Since temperature will influence the relative populations of B*- and B-forms[107], the predisposition towards either conformation by different DNA oligonucleotides with different A-tract lengths will be quantified. Next, the impact of other factors governing B*-form, such as position of A-tract, context of flanking sequences, and nearest-neighbor distribution will also be evaluated.

Correlation between the structure and thermodynamic studies can provide further insights into how B*-form may be stabilized by thermodynamic effects. It is hypothesized that the combination of both thermodynamic and structural studies can enhance DNA structure prediction of A-tract sequences. Further efforts are still required to assign universally appropriate parameter sets of the hybridization thermodynamics for A-tract oligonucleotides to improve the accuracy of secondary structure prediction. Several factors must be taken into consideration. For example, structural information connecting T_m and B*-form may need to be included in NN models. In addition, accurate modeling of the effect of position of the A-tract within a given sequence may be required, as well as the sequence context adjacent to the A-tract. Such refinement is necessary, not only to predict the threshold values for secondary structure stability, but also to elucidate

the mechanisms that control the formation of secondary structures associated with A-tracts.

1.8 Thesis Organization

This chapter highlights the background information relating B*-form with A-tract sequences and covers the theoretical aspects of the spectroscopic methods used to probe factors modulating the non-canonical DNA conformation induced by A-tracts. Chapter 2 provides a description of the materials and methods used in this work. In Chapter 3, a detailed discussion, based on the experimental results obtained, will focus on the factors governing the propensity for B*-form structure and whether or not a correlation exists between the B*-form structure and its thermodynamic properties. Chapter 4 provides the some insights into the effect of conformation on the overall A-tract structure, induced by the incorporation of locked nucleic acid (LNA) bases. Finally, Chapter 5 summarizes the current results and provides some possible guidelines for further investigating the stability and dynamics of B*-form structure.

Chapter 2

Materials and Methods

2.1 Introduction

The materials and methods used in the experiments performed in this work will be presented in this chapter. The rationale for the design of A-tract DNA oligonucleotides used will be discussed. In this study, the spectroscopic techniques, ultraviolet (UV) absorbance and circular dichroism (CD), used to monitor changes in absorbance and chirality in the UV region, will be discussed.

2.2 DNA Oligomer Design

The rationale for our oligomer design is based on assessing the structural influences of A-tracts on the extent of B*-DNA formation in a systematic fashion and to determine if a correlation exists between thermodynamic stability and these structural findings. In Table 2.1, the five different sets of short DNA oligomers are summarized. These were designed to be 12 base pairs in length to ensure that duplex formation proceeds in a two-state manner. The A-tract site of each oligonucleotide shown in Table 2.1 is underlined for clarity.

Set I oligomers, d(TATTATAATATA) and $d(A)_{12}$, were used as control sequences to represent B-form and B*-form, respectively.

Set II represents the PAM group of sequences, which contain a centrally located A_7-tract site of general sequence $(dA)_n$, where n = 3, 4, 6, 8, and 10, flanked on either side by AT and TA base pairs. By varying the length of the A-tract, this set of sequences

serve to investigate the effects of A-tract length on the extent of formation of B*-type helix.

The minor groove at the 5'end of A-tracts is wide and it gradually narrows towards the 3'-end. The gel mobilities of sequences adjacent to the 3'-end, rather than the 5'-end, of an A-tract have been shown to be indistinguishable from one another[167]. Therefore, set III oligomers (hereafter termed PAE sequences) were designed to position the A-tract site at the 3'-end of the sequence, with AT and TA base pairs flanking the 5'-end of the A-tracts. The A-tract lengths for the PAE sequences were designed to be the same as those of PAM sequences to enable direct comparisons between PAM and PAE sequences for the evaluation of positional effects of A-tract on the amount of B*-type helix formation.

Set IV which consisted of PAM 4b and PAM 4c were designed to have the same number of consecutive adenine runs as PAM 4. With this design, any differences in the nearest neighbor contributions to DNA stability and/or subtle structural/conformational deviations from the standard B-form between duplexes of the same length should be attributable to difference in only flanking sequence contexts.

It is well-established that sugar pucker of locked nucleic acids (LNA) is locked in a C3'-*endo* conformation and thus yields an A-form duplex. The locked ribose conformation enhances base-stacking and backbone re-organization, which significantly increases the thermal stability of oligonucleotides. Therefore, Set V was designed to examine the influence of the presence of the conformationally biased locked bases towards the overall A-tract structure through a direct comparison between the LNA:DNA duplexes (ALNA1 and ALNA2) and their respective natural analogs (EE07 and EE08).

The structures formed by DNA sequences containing A-tracts were characterized by UV absorbance and circular dichroism methods, which will be addressed in the following sections.

Table 2.1: DNA oligomers used in this study were designed to address the issues relating to factors that determine the propensity for B*-form conformation. A-tracts are underlined for clarity. These oligomers are grouped into four different sets: set I oligomers were used as control sequences for comparative purposes; set II oligomers contain centrally located A-tract sites; set III oligomers contain A-tract sites which are positioned at the 3'-end; set IV oligomers were used to determine the influence of neighboring base pairs which flank the A-tract; set V oligomers were evaluated for conformational effects on the A-tract structure.

Set	Name	Sequence (12-mers)	T_m (°C)
Set I	NA01	d(TATTATAATATA)	36.5
	EE07	d(AAAAAAAAAAAA)	47.7
Set II	PAM 3	d(ATTATAAATATT)	37.8
	PAM 4	d(TATTAAAATTAT)	42.6
	PAM 6	d(TATAAAAAATAT)	42.8
	PAM 8	d(TTAAAAAAAATT)	43.4
	PAM 10	d(TAAAAAAAAAAT)	45.5
Set III	PAE 3	d(TATTATAATAAA)	36.9
	PAE 4	d(TATTATATAAAA)	35.5
	PAE 6	d(TATTATAAAAAA)	39.5
	PAE 8	d(TATTAAAAAAAA)	40.2
	PAE 10	d(TTAAAAAAAAAA)	41.2
Set IV	PAM 4	d(TATTAAAATTAT)	42.6
	PAM 4b	d(TAATAAAATAAT)	40.0
	PAM 4c	d(ATATAAAATATA)	38.9
Set V	EE07	d(AAAAAAAAAAAA)	47.7
	ALNA1	d(AAA^L AAA^L AAA^L AAA)	52.3
	EE08	d(TTTTATAATAAA)	36.2
	ALNA2	d($TTT^L TAT^L AAT^L AAA$)	43.1

2.3 Buffer and Sample Preparation

The pH 7.0 buffer solution consisted of 1 M NaCl, 10 mM Na_2HPO_4, and 1 mM Na_2(EDTA). EDTA chelates divalent or trivalent cations that nucleases need to degrade DNA. EDTA also prevents the binding of these cations to DNA, which may adversely affect the melting process of the DNA during the experiments. Sodium chloride was used to adjust the ionic strength and total Na^+ concentration. The buffer was filtered through a 0.2 μm syringe filter to remove microbes and dust particles.

DNA oligomers were generously contributed by C. A. Haynes, who purchased them from Integrated DNA Technologies, Inc. (Coralville, IA, USA) and were used in this work without further purification. The initial concentrations were estimated based on UV absorbance at 260 nm[125]. Stock solutions of the double-stranded forms were prepared by mixing equimolar amounts of complementary strands. Samples of 5.0 μM DNA oligonucleotides were then prepared by diluting an aliquot of the stock solution with the buffer solution. Prior to use, each sample was annealed by heating to 80 °C, followed by cooling to room temperature at a rate of 0.5°C/min.

2.4 UV Absorbance Measurements

For the purpose of obtaining thermal difference spectra (TDS), the protocols for obtaining UV absorbance measurements closely follows the method described by Mergny et al[128]. Absorbance measurements were conducted using a Varian Cary 4000 UV-Vis double-beam spectrophotometer, equipped with a Peltier temperature control accessory. Using 1 cm pathlength cells, the UV absorbance measurements were acquired at the temperatures that correspond to the fractions of unfolded and folded DNA are $\leq 1\%$ and $\geq 95\%$, respectively, as predetermined calorimetrically by members of the C. A. Haynes

laboratory. In other words, the T_m of the DNA must lie between these two temperature values. For all the samples, the choice of the upper and lower temperature was $\geq 75°C$ and $\leq 15°C$, respectively. UV absorbance spectra were collected at every 1 nm data interval with a scan speed of 600nm/min for the wavelength range of 240 – 340 nm. TDS were obtained by subtracting the low temperature spectrum from the high temperature spectrum.

2.5 Circular Dichroism Measurements

CD spectra were acquired using a JASCO 810 Spectropolarimeter equipped with Peltier devices. All measurements were obtained in a nitrogen environment to remove oxygen from the instrument because the high intensity xenon light converts oxygen to ozone which destroys the optics in the CD instrumentation. The DNA oligomers were prepared in buffer to a final total strand concentration of 25 μM. Each oligomer sample was placed in a 2.0 mm pathlength cuvette (Suprasil, Hellma, UK). The solution was heated to 75 °C for 10 minutes and slowly cooled to 15 °C. Samples were allowed to equilibrate at the particular temperature studied for 15 minutes prior to the measurement.

The spectropolarimeter was scanned from 200 nm to 340 nm at a scan rate of 50 nm/min. Data points were acquired for every 1 nm with a response time of 4 seconds. All CD data were the average of five accumulations and were buffer-subtracted. To ensure little or no instrumental drift, baselines were recorded both before and after recording the sample spectrum and averaged.

Chapter 3

Results and Discussion

3.1 Thermal Difference Spectra by UV Measurements

Figure 3.1A shows the UV absorbance spectra of double-stranded and single-stranded forms of $d(A)_{12}$ at 15°C and 75°C, respectively. The change in UV light absorption during DNA denaturation is attributed to the change in ε between the single-stranded and double-stranded forms. The major peak occurring at ~ 260 nm is ascribed to $\pi \rightarrow \pi^*$ transitions[59, 61]. The increased absorbance at high temperature indicates that the base-stacking interactions in the native structure are disrupted when the oligomer sample is heated. The subtraction of the low temperature spectrum from the high temperature spectrum resulted in the TDS displayed in Figure 3.1B, characterized by a maximum peak at 260 nm and a slight shoulder located at ~ 295 nm. While the difference absorbance band at 260 nm again reflects $\pi \rightarrow \pi^*$ transitions, the slight shoulder at ~295 nm is indicative of the presence of $n \rightarrow \pi^*$ transitions[59, 61]. The shapes of all the resulting TDS are quantitatively similar to that of $d(A)_{12}$ (Figure 3.1B) since all of the oligonucleotide samples used in this study have 100% AT content. This finding is in agreement with a previous suggestion that TDS shapes depend on base composition and are useful in reflecting the subtleties of base-stacking interactions[110]. For example, Figure 3.2 compares the TDS of the control sequences $d(A)_{12}$ (EE07) and d(TATTATAATATA) (NA01). Figure 3.2 shows how the two TDS curves differ, with $d(A)_{12}$ having a substantially higher intensity than that observed for d(TATTATAATATA). Since the $\pi \rightarrow \pi^*$ and $n \rightarrow \pi^*$ transition moments are perpendicular and parallel, respectively, to the helix axis, increased

stacking resulting from the formation of a folded structure of $d(A)_{12}$ may result in hyperchromism[59, 110]. The differences between the TDS for all the samples in this study are mainly characterized by the exact location and intensities of the maximum peak, as summarized in Table 3.1. As shown in Table 3.1, the wavelength maxima of the heteropolymeric d(TATTATAATATA) and the homopolymeric $d(A)_{12}$ sequence are 259 nm and 263 nm, respectively. This result is in agreement with findings of Mergny *et al.* that the peak maxima positions of sequences containing alternating AT motifs are shifted towards shorter wavelengths compared to sequences with A_nT_n blocks[110]. This observation can be explained by the differences in base-stacking interactions that stabilizes the formation of different conformations, i.e. B*-form or B-form, as a result of different interactions between the A-tract region and the neighboring sequences.

The plot shown in Figure 3.3 reveals that the difference in absorbance at 260nm increases as a function of A-tract length in the sequences studied. The nature of the observed trend for PAM sequences exhibits a significant increase in intensities going from n = 3 to n =6, where n is the number of consecutive adenines, but increases slowly as the A-tract length approaches that of $d(A)_{12}$ (Figure 3.3). Overall, PAM sequences displayed an additive behavior where the intensity of the TDS band at 260 nm increased in a near-linear fashion over the range of lengths examined. In the case of PAE sequences, the intensities increased going from n = 3 to n = 5, with n=6 having the greatest intensity. However, when n is increased to 8 and 10 consecutive adenines, the intensities decreased. This observation found for PAE sequences could result from base-stacking interactions due to narrowing of the groove within the A-tract being most efficient after approximately six consecutive adenines[111], but declining thereafter.

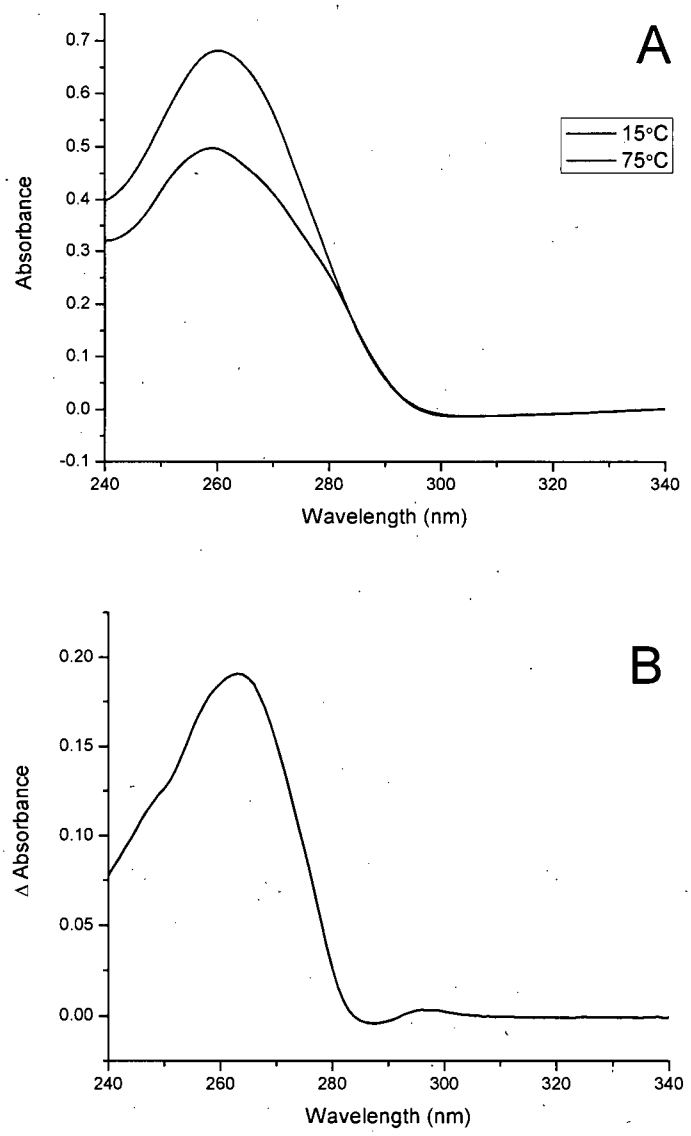

Figure 3.1: Thermal denaturation of the control sequence $d(A)_{12}$ (EE07) monitored by UV absorbance measurements. (A) Comparison of the UV absorbance spectra collected at 15°C (blue line) and 75°C (red line). The major peak at 260 nm reflects the presence of $\pi \rightarrow \pi^*$ transitions as a result of base-stacking interactions. (B) Thermal difference spectrum of poly(dA)·poly(dT) (black line) results from the subtraction of the UV absorbance spectrum at 15°C from the spectrum at 75°C.

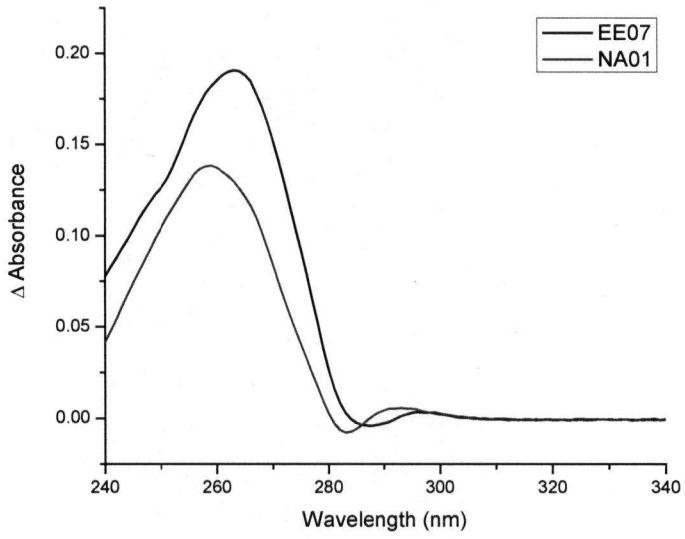

Figure 3.2: Comparison of the UV absorbance difference spectral signatures of the homopolymeric $d(A)_{12}$ (EE07) and heteropolymeric d(TATTATAATATA) (NA01) sequences. The former DNA sequence is representative of a B*-form conformation, whereas the latter is assumed to adopt B-form conformation.

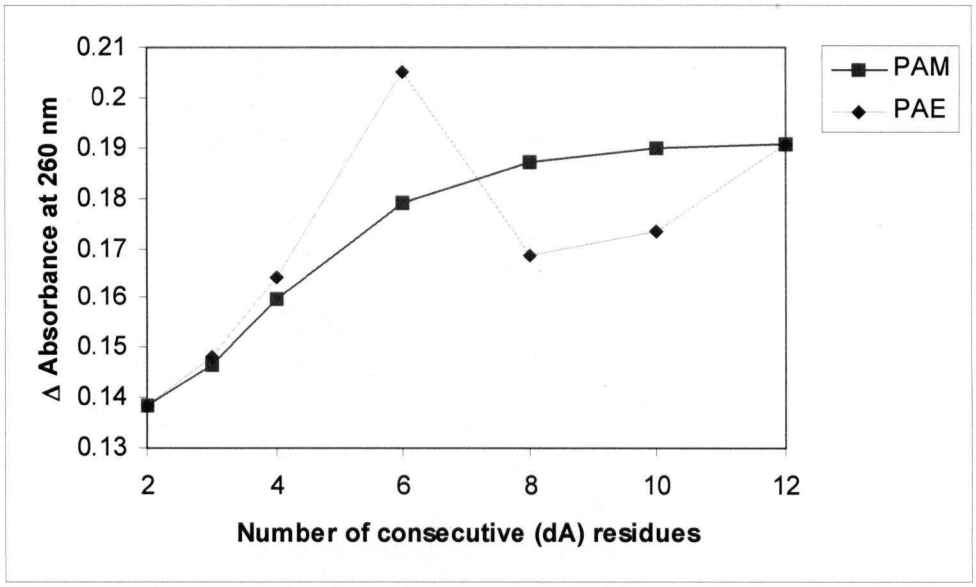

Figure 3.3: Correlation between the ~260 nm peak intensities of the UV difference spectra as a function of A-tract length. The Δ absorbance values on the y-axis are obtained from the difference between the high (75°C) and low (15°C) temperature UV absorbance spectra scanned at 260 nm. A-tract length is determined from the number of consecutive adenine residues within the A-tract site.

Table 3.1: The length and positional effects of A-tracts on the λ_{max} and peak intensities at λ_{max} of the UV absorbance difference spectra.

Name	Sequence (12-mer)	λ_{max}[b] (nm)	Differential absorbance intensity at λ_{max}[c]	Other peaks/features
NA01[a]	d(TATTATAATATA)	259	0.138	*, -
EE07[a]	d(AAAAAAAAAAAA)	263	0.190	**
PAM 3	d(ATTATAAATATT)	263	0.146	*
PAM 4	d(TATTAAAATTAT)	263	0.160	**
PAM 6	d(TATAAAAAATAT)	263	0.179	**
PAM 8	d(TTAAAAAAAATT)	263	0.187	**
PAM 10	d(TAAAAAAAAAAT)	263	0.189	**
PAE 3	d(TATTATAATAAA)	259	0.148	**
PAE 4	d(TATTATATAAAA)	259	0.164	**
PAE 6	d(TATTATAAAAAA)	257	0.205	**
PAE 8	d(TATTAAAAAAAA)	258	0.168	**
PAE 10	d(TTAAAAAAAAAA)	258	0.173	**

- indicates negative peak 283 nm
* indicates shoulder located between 287 – 305 nm
** indicates shoulder located between 290– 300 nm
[a] Control sequences
[b] Standard deviations for λ_{max} at 260 nm is ± 2 nm
[c] Standard deviation for differential absorbance intensities at 260 nm is 0.020

3.2 Temperature-Dependent CD Spectra

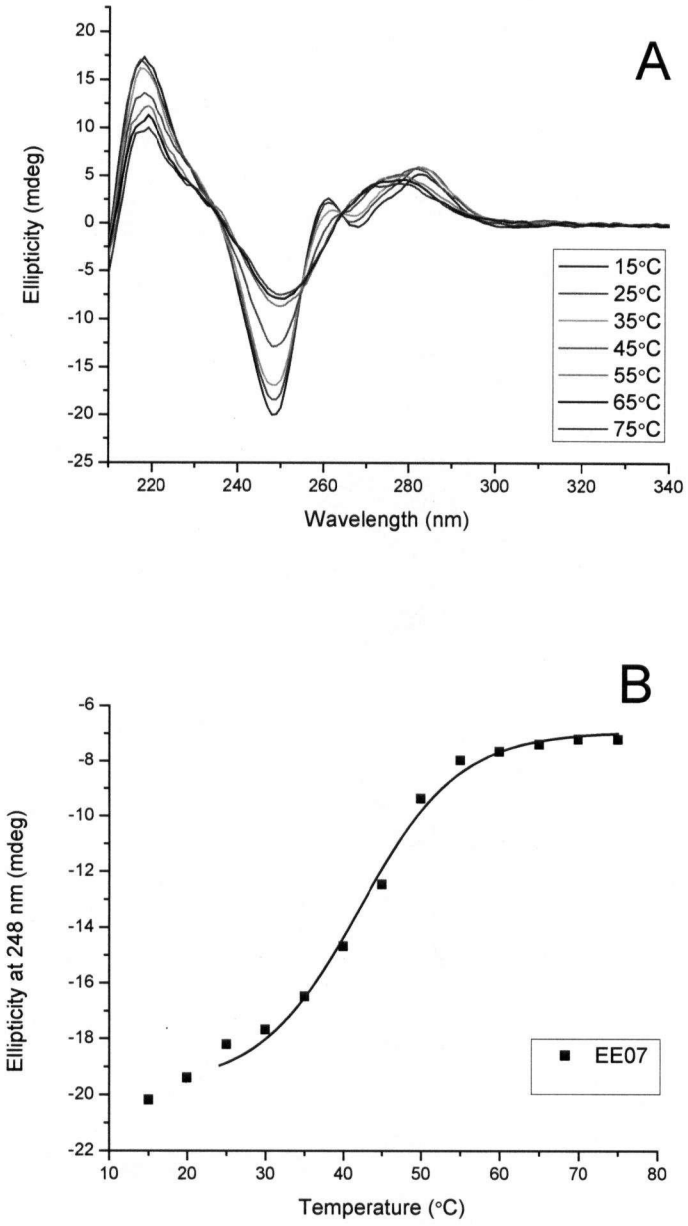

Figure 3.4: Thermal denaturation of $d(A)_{12}$ (EE07) monitored by CD spectroscopy. (A) The CD spectra of $d(A)_{12}$ (EE07) over a temperature range of 15°C to 75°C. The decrease in ellipicity at elevated temperatures above the melting temperature of $d(A)_{12}$ (49.3°C) reflects a decrease in the level of secondary structure. (B) The change in ellipticity at 248 nm with temperature. The solid curve represents the best fit line of the data from 25°C to 75°C, resulting in a melting curve that illustrates the two-state melting behaviour by which the process of denaturation proceeds. The melting behavior of the oligomer at temperatures below 25°C is often referred as a pre-melting transition[113].

Figure 3.4A shows detailed structural information provided by the CD spectra of $d(A)_{12}$ obtained over a series of temperatures ranging from 15°C to 75°C. Changes in the shape and magnitude of the CD intensity extrema reflects progressive disruption of base-stacking and base-pairing interactions as the temperature increases from 15°C to 75°C. At temperatures below the melting temperature of $d(A)_{12}$ (49.3°C), the CD spectra of the duplexes are similar, but not identical. As the temperature increases beyond the melting temperature, more dramatic changes appear in terms of the magnitude and the shape of the peaks at 220 nm, 260 nm, and 280 nm, as well as the trough at 248 nm. These spectroscopic changes suggest that the duplexes initially are structurally or conformationally different at low temperatures and become structurally or conformationally similar at temperatures above the melting temperature[112]. At higher temperatures, the bases have a random orientation relative to one another, resulting in the decrease in ellipticity of the peaks and trough over the wavelength region studied. Also seen in Figure 3.4A is the presence of an isoelliptic point located at 264 nm, which indicates a two-state transition between the double-stranded and single-stranded states with no intermediate steps over the entire temperature range studied[113, 114].

It is clear from the CD spectral data that the conformation adopted by the oligomer sample is dependent on temperature, as the relative peak magnitudes and shapes change with temperature.

At the appropriate wavelength, CD appears to represent the melting curve of the DNA oligomer. The largest temperature-dependent intensity change occurs at 248 nm (Figure 3.4A). Figure 3.4B illustrates the resulting plot of a CD melt performed at 248 nm reflects a sigmoidal curve which is qualitatively similar to a typical melting curve

obtained by UV measurements at 260 nm. This indicates that CD melting studies may also be used to analyze the thermal stability of DNA oligomers.

3.3. CD Spectral Characteristics of B*-form of A-tract Structure

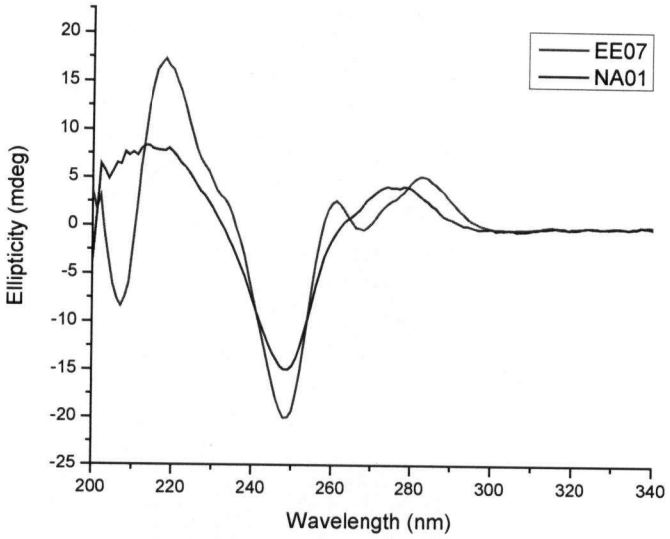

Figure 3.5: CD spectrum of $d(A)_{12}$ (EE07, red line) exhibiting B*-form spectral characteristics. The CD spectrum of B-form d(TATTATAATATA) (NA01, blue line) is shown for comparison . The CD spectra of EE07 and NA01 are measured at 15°C and 10°C, respectively.

Structurally, the heteropolymeric d(TATTATAATATA) (NA01), being in the classical B-DNA conformation, is significantly distinct from the homopolymeric $d(A)_{12}$ (EE07) , which adopts the B* conformation[115, 116]. Structural differences between the two oligomers are reflected, in particular, in the unusually high torsional rigidity of the homopolymeric $d(A)_{12}$ compared to the mixed d(TATTATAATATA) sequence[117-119].

Figure 3.5 compares the CD spectral features between $d(A)_{12}$ (EE07) and d(TATTATAATATA) (NA01), which are used as reference B*-form and B-form structures, respectively. The sequence $d(A)_{12}$ displays a CD spectrum with several

characteristic CD bands located at 209 nm, 220 nm, 248 nm, 261 nm, and 285 nm (red line). In contrast, the CD spectrum of d(TATTATAATATA) (blue line) indicates a conformation expected of a normal B-type helix[120], as evidenced by the absence of a ~ 260 nm band and its 'conservative' character composed of two bands at 248 nm and 280 nm of negative and positive ellipticity, and of nearly equal rotational strength (blue line). This is in good qualitative agreement with literature findings[121–123]: B-form of DNA have a positive ellipticity maximum at 260 nm, a weaker negative band at 250 nm, and a strong negative band at about 210 nm; B-form is defined by CD spectral characteristics of a null near 260 nm, with a broad positive peak in the region of 280 nm and a negative ellipticity maximum near 250 nm. The bands located near 258 nm and 272 nm have previously been assigned to adenine and thymine, respectively[124]. The CD peak at ~ 260 nm for the $d(A)_{12}$ (EE07) spectrum is particularly distinct compared to the B-form CD spectrum of d(TATTATAATATA) (NA01). Thus, the 260 nm CD peak may reveal structural information specific to A-tracts, particularly the formation of B*-form structure, and can be attributed to adenine-adenine stacking. The absence of a 260 nm CD signal and a significant difference in the overall CD spectral features of d(TATTATAATATA) (NA01) mainly results from the absence of A-tracts. This comparative study of the two control sequences to distinguish between B*-form and B-form is required to evaluate whether A-tracts can produce a distinguishable fine structure in the CD of other sequences containing A-tracts (Set II, III, and IV, Table 2.1).

3.4 CD Difference Spectra

In section 3.1, the analysis of the UV absorbance results for different sequences is mainly based on the TDS plots. In the same fashion, the CD difference spectra for all the oligonucleotides used in this study will be generated. According to an earlier discussion by Greve et al., factors such as base-to-backbone and base-base interactions contribute to a smaller extent to the difference spectrum than to an original CD spectrum as they are largely subtracted[114]. Difference CD spectra are better resolved than the original CD spectra and mainly reflect interstrand interactions since intrastrand interactions are largely subtracted. Thus, the advantage of using CD difference spectra lies in their simplicity and subsequent ease of interpretation[114]. In sections that follow, it will be shown that the CD difference spectra of set II, set III, and set IV sequences typically have a positive maximum at 248 nm and a global minimum at 260 nm. Having discussed the overall CD spectral features of conformations of B*-form, we will now address the details of the conformational perturbations induced by the A-tract site as a function of the A-tract length and position within duplex DNA. The impact of the base pairs neighboring the A-tract site will also be discussed.

3.4.1 Analysis of PAM sequences

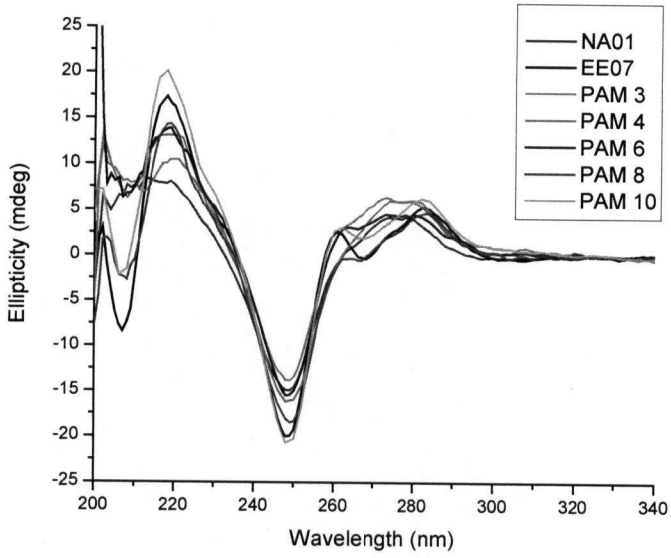

Figure 3.6: CD spectra at 15°C of PAM sequences with different A_n-tract lengths (where n = 3, 4, 6, 8, and 10). The A-tract is located within the central portion of the 12 bp long sequence.

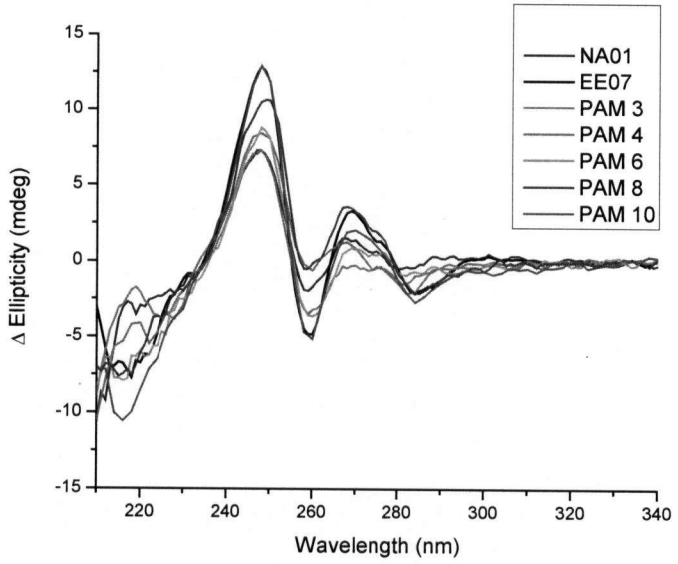

Figure 3.7: CD difference spectra for PAM sequences with various A_n-tract lengths, where n = 3, 4, 6, 8, and 10. These spectra are generated by subtracting the CD spectrum at 15°C from the CD spectrum at 75°C. The CD difference spectra of the control sequences $d(A)_{12}$ (EE07) and d(TATTATAATATA) (NA01) are included for comparison.

The low temperature CD spectra for the PAM series with A_n-tract where n = 3, 4, 6, 8, and 10 are shown in Figure 3.6. These spectra are characterized by peaks centered at 220 nm, 260 nm and between the region of 270 – 280 nm, as well as troughs located at 208 nm and 248 nm. The overall trends of the low temperature CD spectra suggest that the base-stacking interactions, as indicated by the increase in peak height and the increase in trough depth, becomes larger as the length of the A-tract increases.

The low temperature CD spectra of d(TTAAAAAAAATT) (PAM 8) and d(TAAAAAAAAAAT) (PAM 10) resembles the reference B*-form CD spectrum of $d(A)_{12}$ (EE07), as indicated by the similarity in the shape of the ~ 260 nm band. Nevertheless, some differences occurring in the region of 270 – 280 nm between the CD spectra of EE07, PAM 8, and PAM 10, may be attributed to the influence of the thymine residues located at the 5'- and 3'- ends of the duplex. The shape of the low temperature CD spectra for d(ATTATAAATATT) (PAM 3), d(TATTAAAATTAT) (PAM 4), and d(TATAAAAAATAT) (PAM 6) approaches that of a B-form CD spectrum of d(TATTATAATATA) (NA01), as indicated by the formation of a broad CD band in the region between 270 - 280 nm. The intensity of the CD band located at 260 nm, which reflects the contribution from the adenine bases[122], increases as a function of A-tract length. It is interesting to note that this particular trend is also reflected by the band at 220 nm. The intensity and the shape of all the CD bands are distinct for all PAM oligomers, possibly due to the structural differences related to the relative amount of B*-form adopted depending on the sequence context of base pairs neighboring the A-tract site.

Figure 3.7 compares the CD difference spectra of the series of PAM sequences to further evaluate the extent of B*-conformation formed due to A-tract length effects. Compared to other PAM sequences, the CD difference spectrum of PAM 10 bears the closest resemblance to EE07 in terms of the shape and intensity of the bands at 248 nm and 260 nm. However, the difference between PAM 10 and EE07 occurs in the band in the region between 270 – 280 nm, strongly suggestive of either a $\pi \rightarrow \pi^*$ transition on adenine or $n \rightarrow \pi^*$ transition on thymine[114]. In addition, the peak at ~ 270 nm is less pronounced in PAM 10 compared to EE07. This possibly indicates that the destabilizing feature of TA base step within the sequence[125] causes the adenine bases within the A-tract to be slightly less efficiently stacked in PAM 10 compared to EE07[126, 127]. The generally observed increases in intensities for both the peaks and troughs in the CD difference spectra for the PAM series are consistent with increasing base-stacking interactions as the length of the A-tract increase.

There is no clear correlation between CD difference band intensities at 260 nm and A-tract length. However, the CD difference band intensities at 248 nm increase in a non-linear fashion with the length of contiguous adenine residues within the A-tract, as seen in Figure 3.10. As the length dependence approaches a maximum value, the ellipticity approaches that of EE07 slowly, in agreement with the finding by Gudibande *et al*[126]. In general, the difference in ellipticity at 248 nm derived from the CD difference spectra presumably reflect the effect of A-tract length on the overall conformation of a given oligomer sequence.

3.4.2 Analysis of PAE sequences

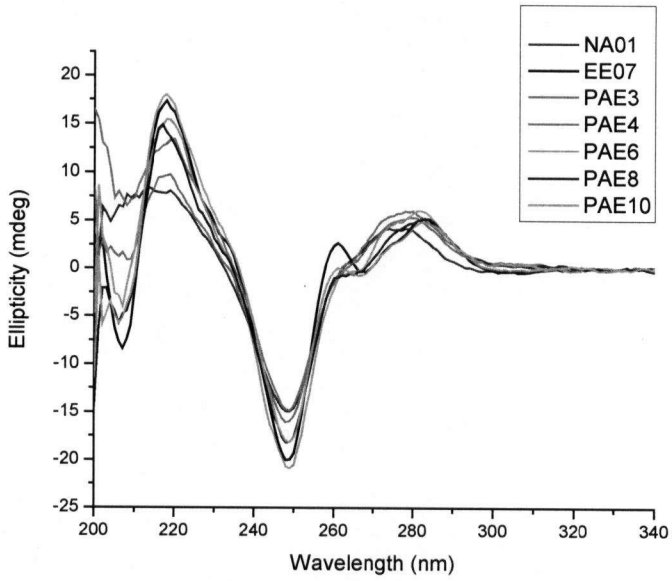

Figure 3.8: CD spectra at 15°C of PAE sequences with different A_n-tract lengths (where n = 3, 4, 6, 8, and 10). The A-tract is located at the 3'-end portion of the 12 bp long sequence.

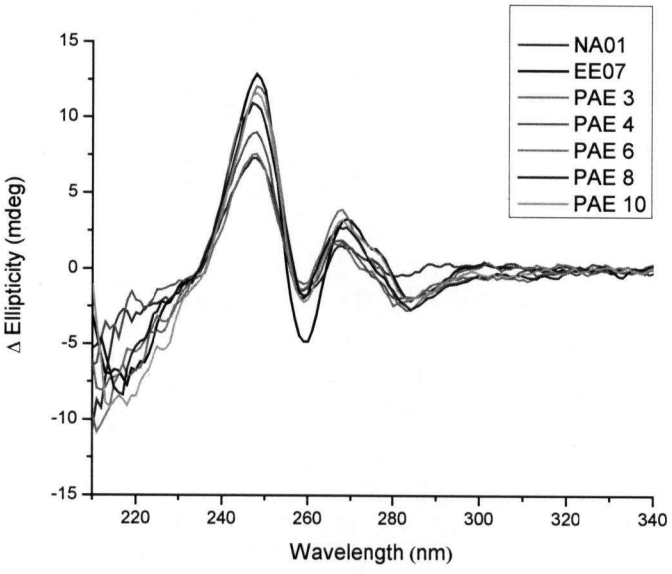

Figure 3.9: CD difference spectra for PAE sequences with various A-tract lengths, n, where n = 3, 4, 6, 8, and 10. These spectra are generated by subtracting the CD spectrum at 15°C from the CD spectrum at 75°C. The difference spectra of the control sequences $d(A)_{12}$ (EE07) and d(TATTATAATATA) (NA01) are included for comparison.

Figure 3.8 shows a comparison of the low temperature CD spectra of the PAE series of oligomers. The structures formed by the PAE series show a lower tendency towards exhibiting the B*-form spectral characteristics as the A-tract lengthens. For all the PAE sequences, the CD spectra remain relatively unchanged in terms of the magnitude of the ellipticity at 260 nm while differing substantially at the 220 nm peak and the 248 nm trough. This implies a lower tendency towards adopting B*-form structure for PAE sequences relative to the results seen for PAM sequences.

Figure 3.9 shows the CD difference spectra for PAE sequences. Here, the CD difference band at 248 nm displayed a general increase in intensity with an increase in A-tract lengths of PAE sequences. In contrast to PAM sequences, the intensity of ~ 260 nm positive peak is somewhat less enhanced for PAE sequences. Thus, end effects did not significantly affect the spectral features of the oligonucleotides. Despite the existence of longer A-tracts which might be expected to be susceptible to local alteration of the overall conformation, the lack of spectral changes at 260 nm may suggest decreased propensity for the formation of B*-form duplex from the 3'-end junction of the A-tract[128].

Based on the CD difference spectra in Figure 3.9, the peak intensities at 248 nm for PAE sequences are plotted as a function of A-tract length in Figure 3.10. It is interesting to note that this trend for PAE is similar to a corresponding trend observed in UV difference spectra (Figure 3.3), suggesting that the UV transition at ~ 260 nm can be detected by ellipticity at ~ 248 nm. For example, the data point for d(TATTATAAAAAA) (PAE 6) displayed an unexpectedly higher intensity in the CD difference ellipticity at 248 nm compared to d(TATTAAAAAAAA) (PAE 8) and d(TTAAAAAAAAAA) (PAE 10). Like the PAM series, the PAE series of sequences

generally also show considerable differences between the 248 nm intensities of the CD difference spectra as a function of A-tract length.

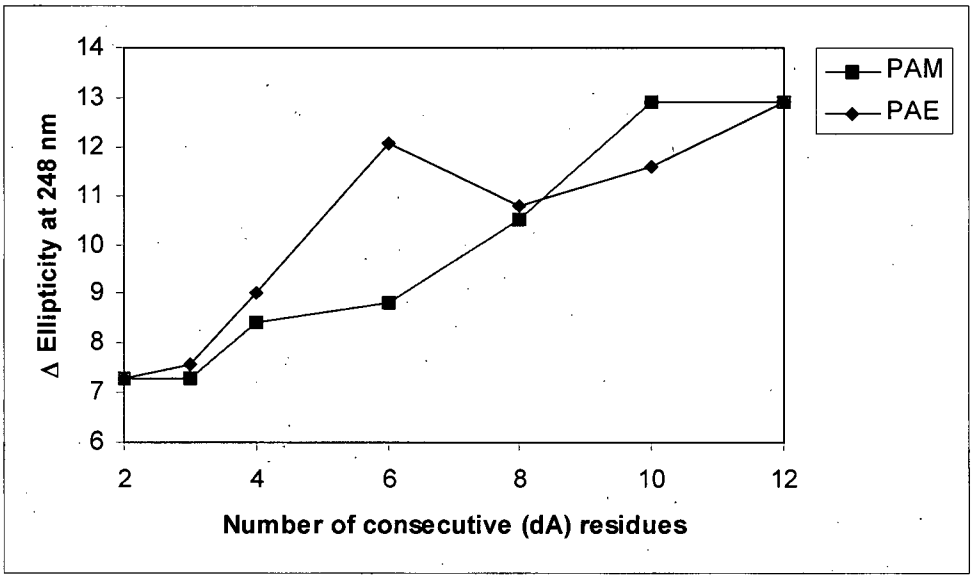

Figure 3.10: The plot of 248 nm peak intensities of the CD difference spectra as a function of A-tract length for PAM (squares) and PAE (diamonds) series. The Δ ellipticity values on the y-axis are obtained from the difference between the high (75°C) and low (15°C) temperature CD spectra at 248 nm. The trend for both series of sequences show that the 248 nm intensities based on the CD difference spectra is useful in providing insight into effects of A-tract length.

3.4.3 Effects of Sequences Flanking the A-Tract

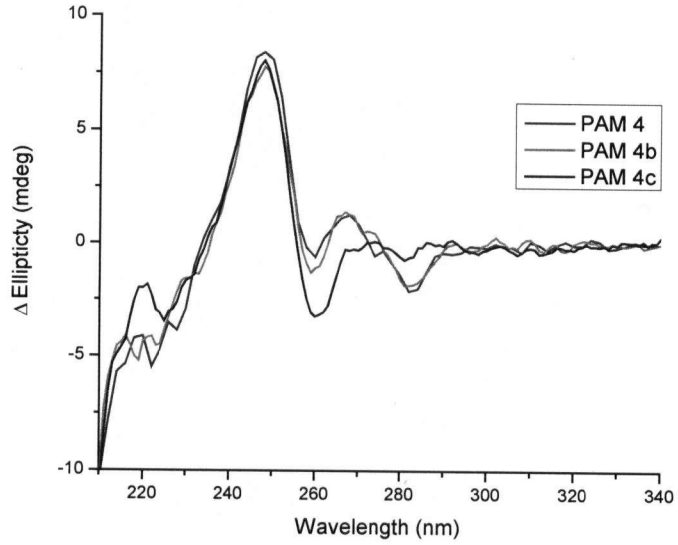

Figure 3.11: Comparison of the CD difference spectra of d(TATTAAAATTAT) (PAM 4), d(TAATAAAATAAT) (PAM 4b), and d(ATATAAAATATA) (PAM 4c) to evaluate the effect of TT, AT and TA base pair steps flanking the A-tract site. These sequences contain the same A-tract length but have different sequence context in the base pairs neighboring the A-tract site.

To properly investigate the influence of flanking sequences on A-tracts, three sequences with the same A-tract length are evaluated. The contrast between the T_m values of sequences d(TATTAAAATTAT) (PAM4) and d(TAATAAAATAAT) (PAM4b) illustrates the presence of a base polarity effect, e.g. AT versus TA, and its influence on thermal stability. When TA base pairs are located adjacent to the A-tract site, towards both 5'- and 3'- directions, the T_m decreased from 42.6°C (PAM4) to 40.0°C (PAM4b). When two TA base pairs flanked both sides of the A-tract as seen in sequence d(ATATAAAATATA) (PAM4c), there is a further decrease in T_m to 38.9°C. The decreasing trend in T_m with the increasing number of flanking TA base pairs is also observed in the corresponding ΔS° and ΔH° values. These results suggest that a TA base

pair adjacent to the A-tract site has a destabilizing effect on the duplex, whereas greater stability is found with flanking TT (= AA) and AT base pairs. These observations strongly agree with previous findings that emphasized the more efficiently stacked AT steps versus TA steps[129, 130]. Crystallography studies have shown that large conformational changes found at the TA and AT steps, especially at junctions of the A-tract and non-A-tract region, can lead to close cross-strand contacts between adenine bases across an AT step and may explain the different behavior of AT versus TA steps in the context of A-tract induced curvature[131].

The structural comparison based on CD difference spectra for PAM4, PAM4b, and PAM4c is illustrated in Figure 3.11. The band at 248 nm does not show significant differences in magnitude for all the sequences that are compared because all three of these sequences have the same A-tract length. This observation confirms that the intensity of the band at 248 nm is dependent on A-tract length.

Knowing that these sequences contain different sequence context in the regions adjacent to the A-tract, the variability revealed in the CD difference band at ~ 260nm may reflect the detailed mutual orientations of these bases adjacent to the A-tract in the helix[67]. The band intensity obtained from the CD difference spectra at ~260 nm decreased in the following order: PAM4c > PAM4b > PAM4, in agreement with the trends in thermodynamically observed results. A possible explanation for the observed results is that the bases flanking the A-tract region may be a determining factor in the preferential stability of the overall conformation of the oligonucleotide. Since the 5' TA step has lower energy of stacking interaction (ΔH = 6.0 kcal/mol) than AT (ΔH = 8.6 kcal/mol)[132], less favorable stacking interaction exist for TA than for AT base steps,

causing the former to be more easily disrupted. This provides additional stabilization energy for the formation of B*-conformation induced by the adenine base-stacking within the A-tract in order to maximize π overlap[133]. Hence, a much more intense negative band at ~260 nm resulted for PAM4c than PAM4 and PAM4b. Overall, these results reveal a relationship between the extent of interaction with neighboring base pairs and the thermodynamic properties of the A-tract containing duplexes. The nature of flanking sequences could make the formation of B*-DNA more or less favorable.

3.5 Quantification of DNA Secondary Structure

Although A-tract length information is conveniently accessed from the intensity of the bands at 248 nm from the CD difference spectra, its relationship to the amount of B*-form is complicated and can be significantly influenced by the effect of flanking sequences. In order to determine what truly determines B*-form content, it should be kept in mind that B*-form is a consequence of compact base-stacking arrangement[24]. Since we know that the sequences with A-tracts forming B*-form structures are characterized by a positive CD signal at ~ 260nm by referral to a reference spectrum, this peak is directly related to the type of secondary structure present and can be used to give an estimate for the relative population of B*-form in the oligomers studied.

Analogous to the method used by Scarlett *et al*[123] for determining the percentage A- or B- form duplex, $d(A)_{12}$ (EE07) is assumed to give the best estimate of 100% B*-form. NA01 is not used to represent 0% B*-form since it has a slight signal at 260 nm, evident from its low temperature CD spectrum and CD difference spectrum. Rather, NA01 will be used qualitatively as a reference B-form spectrum. A "flexrod" baseline, as illustrated in Figure 3.12, for CD_{260} of $d(A)_{12}$ (EE07) is used as a reference baseline for

calculating the relative peak heights of all the other sequences at ~260 nm. The percentage B*-conformer is calculated by taking the ratio of the individual peak heights at ~260 nm over the peak height of EE07. The percentage of B*-form content for both PAM and PAE sequences, listed in Table 3.2, are plotted against A-tract length (expressed as the percentage consecutive (dA) residues), resulting in linear plots seen in Figure 3.13. B*-form content of a DNA duplex increases as a function of A-tract length. A good linear correlation is obtained for both PAM ($R^2 = 0.912$) and PAE ($R^2 = 0.989$) sequences. It should be noted, however, that this method of quantification is merely an estimation of B*-form content because these values are not corrected in terms of fraction DNA melted and the "flexrod" baseline is not the true baseline of the entire spectrum.

Table 3.2: Summary of B*-form content in PAM and PAE sequences. The percentage B*-form for all the sequences are calculated based on the assumption that the control sequence $d(A)_{12}$ (EE07) best represents 100% B*-form.

Name	Sequence (12-mer)	Peak CD_{260} ($\Delta\varepsilon$)	% B*-form
NA01	d(TATTATAATATA)	1.57	16.94
EE07	d(AAAAAAAAAAAA)	9.27	100.00
PAM 3	d(ATTATAAATATT)	2.38	25.67
PAM 4	d(TATTAAAATTAT)	1.60	17.26
PAM 6	d(TATAAAAAATAT)	3.00	32.36
PAM 8	d(TTAAAAAAAATT)	4.80	51.78
PAM 10	d(TAAAAAAAAAAT)	8.76	94.50
PAE 3	d(TATTATAATAAA)	1.95	21.04
PAE 4	d(TATTATATAAAA)	2.88	31.07
PAE6	d(TATTATAAAAAA)	4.15	44.77
PAE 8	d(TATTAAAAAAAA)	5.61	60.52
PAE 10	d(TTAAAAAAAAAA)	6.93	74.76

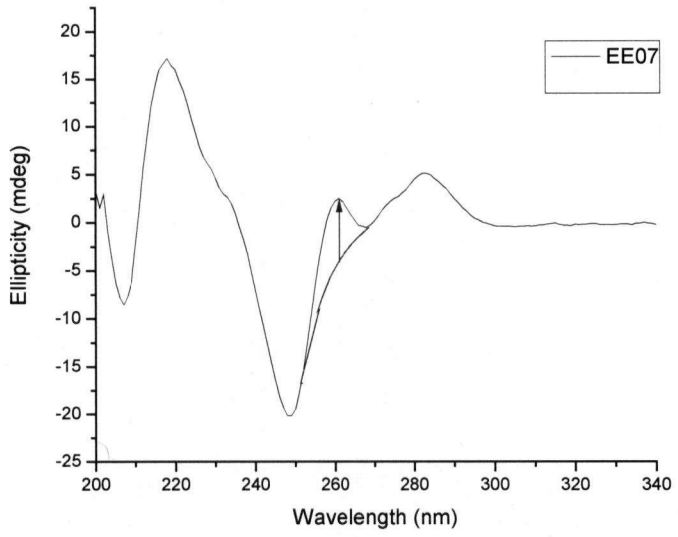

Figure 3.12: An illustration of the "flexrod" baseline (red line) used to obtain the magnitude of the CD signal (red arrow) at 260 nm. The 260 nm CD peak is attributed to adenine base stacking of the A-tract site. Since A-tracts are responsible for the formation of the overall B*-form structure, the magnitude of the 260 nm CD signal is used to estimate the amount of B*-form structure formed.

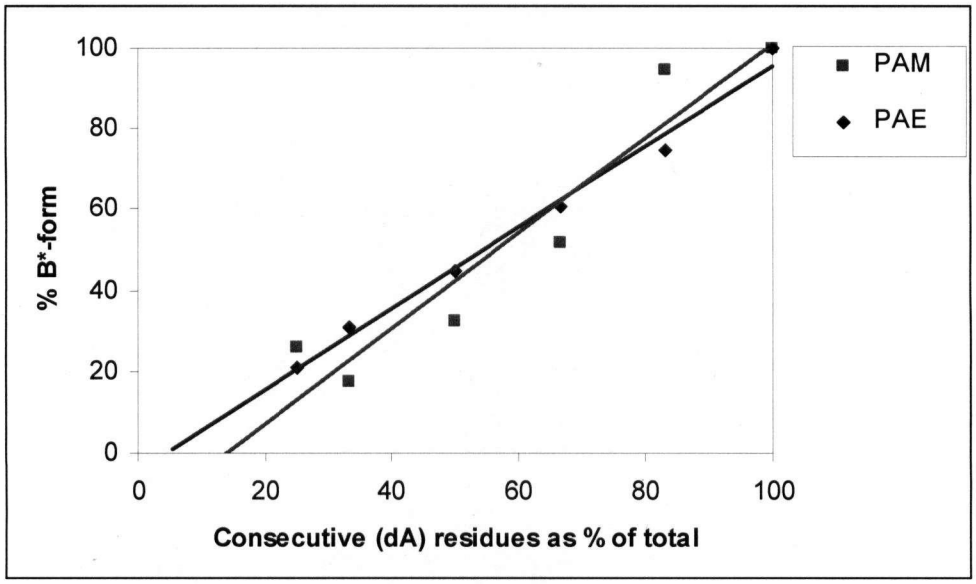

Figure 3.13: Quantification of B*-form content of PAM (squares) and PAE (diamonds) sequences with respect to A-tract length (expressed as consecutive (dA) residues as % of total). The correlation factor, R^2, for PAM and PAE are 0.912 and 0.989, respectively.

3.6 Comparison of Spectroscopic and Thermodynamic Results

3.6.1 Correlation of UV Measurements with Thermodynamic Variables

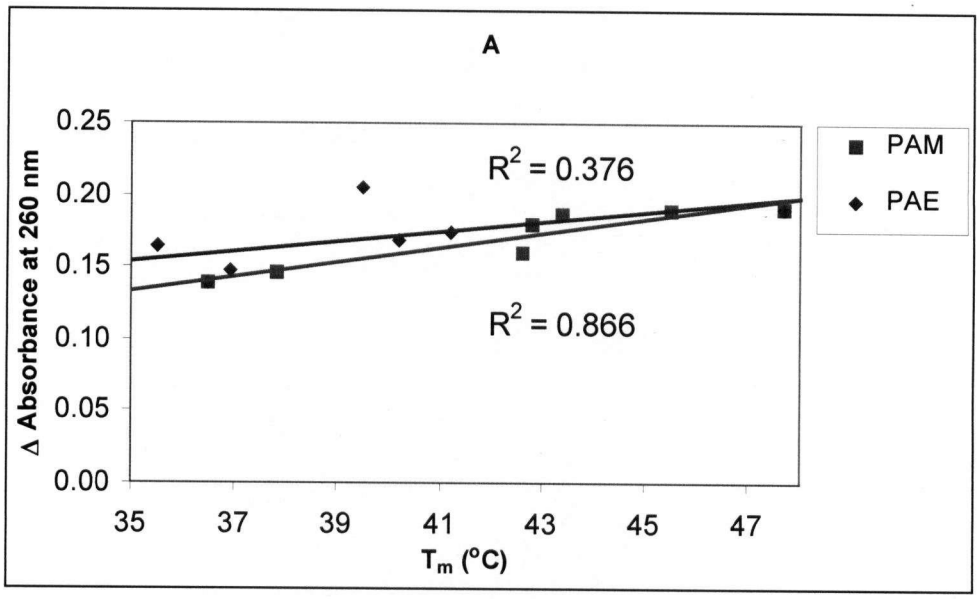

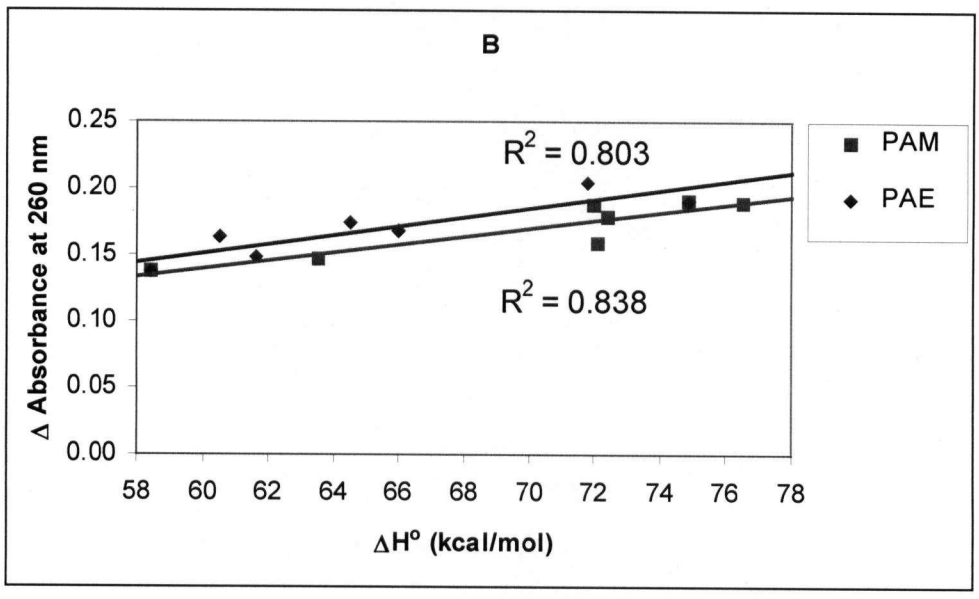

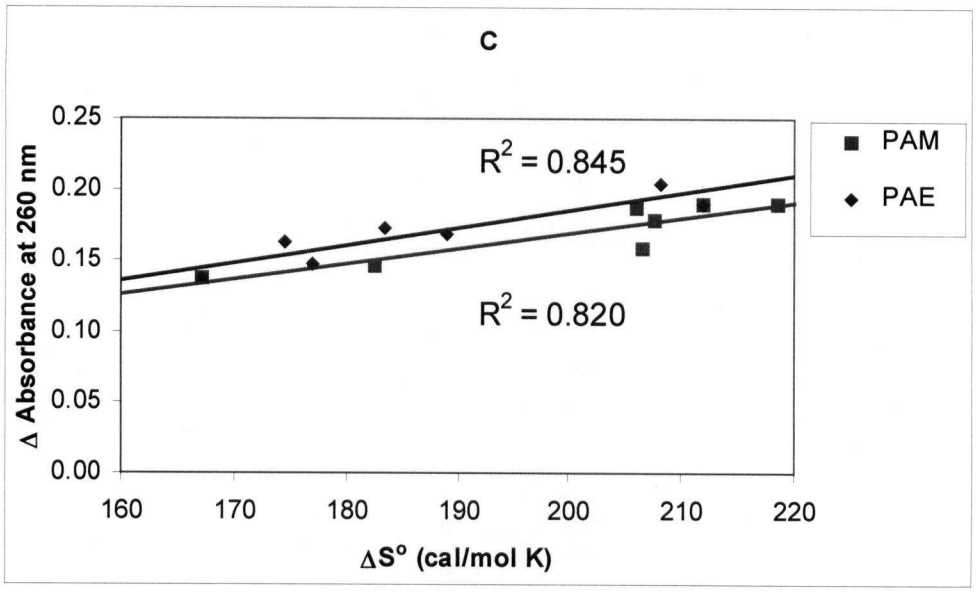

Figure 3.14: Correlation between TDS peak intensities at 260 nm with (A) T_m, (B) ΔH°, and (C) ΔS° for PAM (squares) and PAE (diamonds) sequences. The pink and blue lines represent the best linear fits for PAM and PAE data sets, respectively. The correlation factors for PAM and PAE, respectively, are: (A) R^2 (PAM) = 0.866 and R^2 (PAE) = 0.376, (B) R^2 (PAM) = 0.838 and R^2 (PAE) = 0.803, (C) R^2 (PAM) = 0.820 and R^2 (PAE) = 0.845.

On the basis of TDS spectra obtained by UV measurements, the intensities of the maxima located at ~260 nm reflects the increase in the absorbance of ultraviolet light that accompanies the unstacking of bases upon denaturation of duplex DNA. Correlation of differential absorbance values at 260 nm with T_m (Figure 3.14A), ΔH° (Figure 3.14B), and ΔS° (Figure 3.14C) for PAM and PAE sequences generally show good linear correlations, as indicated by values of $R^2 > 0.8$. An exception is found for the relationship between T_m of d(TATTATAAAAAA) (PAE 6) and its differential 260 nm absorbance value (Figure 3.14A), due to the possibility that there exists a critical A-tract length that most favors B*-like formation, particularly for the case where A-tract is positioned at the 3'end.

3.6.2 Correlation of CD Measurements with Thermodynamic Variables

The thermodynamic parameters, T_m, $\Delta H°$, and $\Delta S°$, for all the oligonucleotides used in this study are tabulated in Table 3.3. These results are obtained through differential scanning calorimetric experiments conducted by Curtis Hughesman of the C. A. Haynes lab. Thermodynamic analysis provides insight into the stability of B*-form formation, thereby complementing the structural evidence of B*-form observed from UV and CD experiments.

Table 3.3: Summary of the thermodynamic variables for DNA sequences containing A-tracts obtained by DSC measurements. Each of the 75 μM samples are suspended in a buffer solution containing 1 M NaCl, 10 mM Na_2HPO_4, and 1 mM Na_2(EDTA) (pH 7.0). (Reproduced with permission from Curtis Hughesman)

Name	Sequence (12-mer)	T_m[a] (°C)	$\Delta H°$ (kcal/mol)	$\Delta S°$ (cal/mol·K)
NA01	d(TATTATAATATA)	36.5 (35.9)[b]	58.4 (76.0)	167.1 (224.4)
EE07	d(AAAAAAAAAAAA)	47.7 (46.3)	74.9 (82.3)	211.9 (236.1)
PAM 3	d(ATTATAAATATT)	37.8 (39.3)	63.5 (77.4)	182.6 (226.2)
PAM 4[c]	d(TATTAAAATTAT)	42.6 (39.8)	72.1 (78.1)	206.6 (228.0)
PAM4b[c]	d(TAATAAAATAAT)	40.0 (39.8)	65.7 (78.1)	188.2 (228.0)
PAM4c	d(ATATAAAATATA)	38.9 (37.6)	58.5 (76.7)	165.8 (225.3)
PAM 6[c]	d(TATAAAAAATAT)	42.8 (39.8)	72.4 (78.1)	207.6 (228.0)
PAM 8	d(TTAAAAAAAATT)	43.4 (44.2)	72.0 (80.9)	206.0 (233.4)
PAM 10	d(TAAAAAAAAAAT)	45.5 (44.2)	76.5 (80.9)	218.5 (233.4)
PAE 3	d(TATTATAATAAA)	36.9 (38.1)	61.6 (77.4)	177.0 (227.1)
PAE 4	d(TATTATATAAAA)	35.5 (38.1)	60.5 (77.4)	174.5 (227.1)
PAE6	d(TATTATAAAAAA)	39.5 (40.4)	71.8 (78.8)	208.1 (229.8)
PAE 8	d(TATTAAAAAAAA)	40.2 (42.5)	66.0 (80.2)	189.1 (232.5)
PAE 10	d(TTAAAAAAAAAA)	41.2 (44.7)	64.5 (81.6)	183.4 (235.2)

[a] Melting temperatures are calculated at the total oligomer strand concentration of 75 μM. Esimated errors in T_m, $\Delta H°$, and $\Delta S°$ are approximately 0.3 %, 15.1 %, and 16.5 % respectively.
[b] The values in parentheses are predicted using the Santa Lucia nearest-neighbor model, whereas the values in non-parenthesis are experimentally determined values obtained from DSC plots.
[c] DNA duplexes with identical nearest-neighbor base pairs.

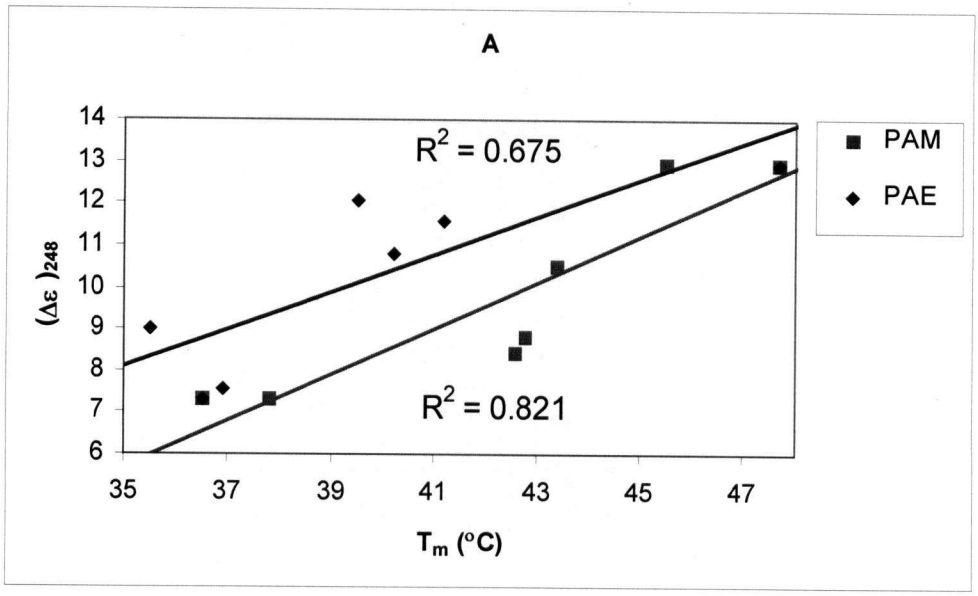
A
14
13
12
11
10
9
8
7
6
$(\Delta\varepsilon)_{248}$
$R^2 = 0.675$
$R^2 = 0.821$
35
37
39
41
43
45
47
T_m (°C)
PAM
PAE

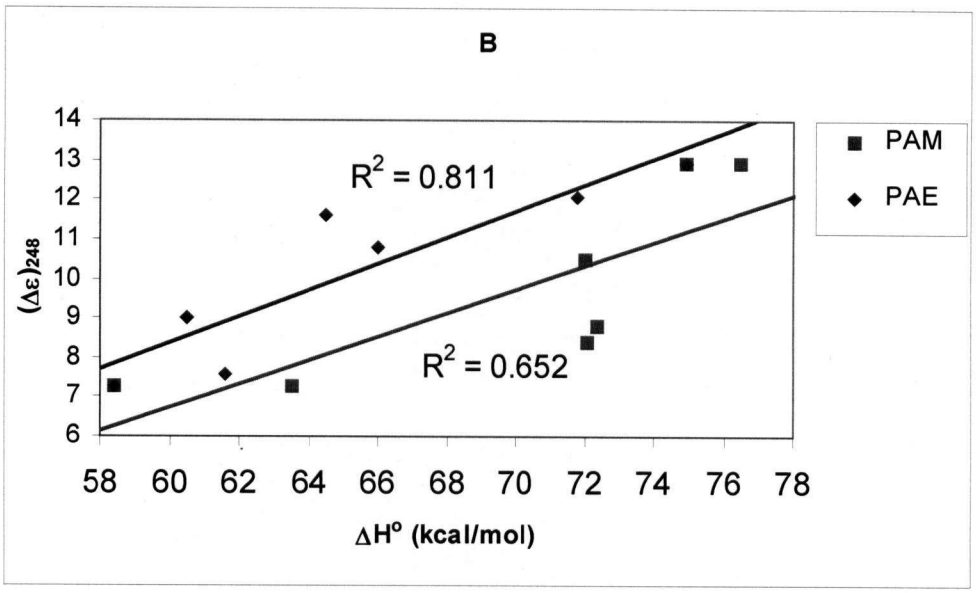
B
14
13
12
11
10
9
8
7
6
$(\Delta\varepsilon)_{248}$
$R^2 = 0.811$
$R^2 = 0.652$
58
60
62
64
66
68
70
72
74
76
78
ΔH^o (kcal/mol)
PAM
PAE

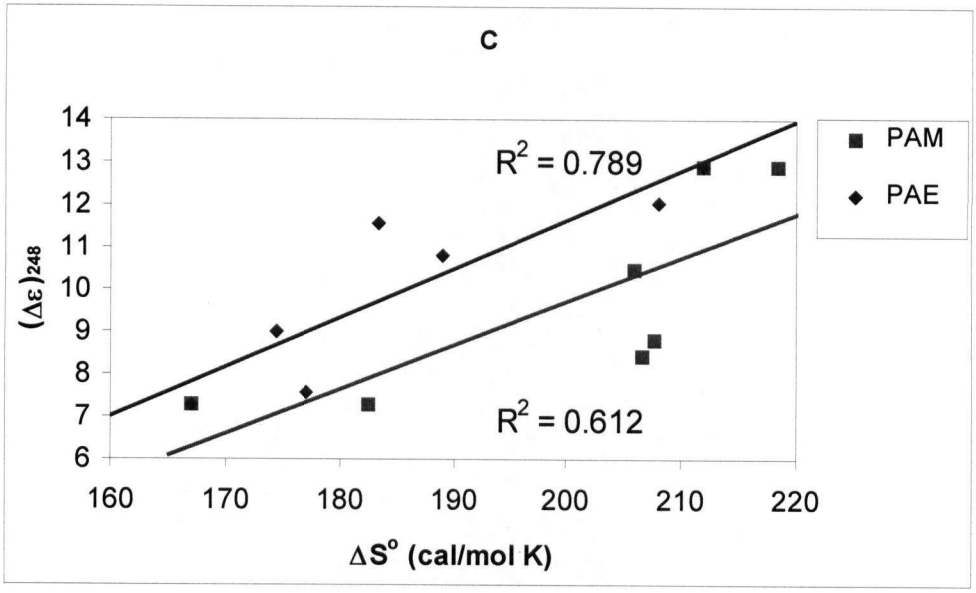

Figure 3.15: Correlation between CD difference spectra peak intensities at 248 nm with (A) T_m (B) ΔH° and (C) ΔS° for PAM (squares) and PAE (diamonds) sequences. The pink and blue lines represent the best linear fits for PAM and PAE data sets, respectively. The correlation factors for PAM and PAE, respectively, are: (A) R^2 (PAM) = 0.821 and R^2 (PAE) = 0.675, (B) R^2 (PAM) = 0.652 and R^2 (PAE) = 0.811, (C) R^2 (PAM) = 0.612 and R^2 (PAE) = 0.789.

The peak intensities at 248 nm obtained from the CD difference spectra of PAM and PAE series of oligomers are plotted against T_m (Figure 3.15A), ΔH° (Figure 3.15B), and ΔS° (Figure 3.15C) in order to observe the correlation between structure and thermodynamic parameters. In each case, the increase in A-tract length induces thermal stabilization as seen with the increase in melting temperature and enthalpy values[134]. ΔH° increases more-or-less in parallel with the adenine content of the A-tract. This observation is reflective of increased base stacking and hydrogen bonding interactions[134, 135]. Overall, the larger entropy values for PAM sequences compared to PAE sequences suggest that the formation of B*-form is more enthalpically favored.

The correlation of difference in ellipticity at 260 nm, $(\Delta\varepsilon)_{260}$, with thermodynamic variables lead to rather inconsistent results with small correlation coefficient values. This

situation illustrates the complexity behind contributions to thermodynamic stability and argues for more careful consideration of sequence effects. DNA sequence effects for the A-tract oligomers in this study can be divided into two groups: (i) sequence effects within the A-tract region, such as the interactions between all the neighboring base pairs, and (ii) sequence effects within the non-A-tract region, such as the differences in nucleotide composition of A-tract flanking sequences, and the influence of the base pairs at the 5'- and 3'-end. Of the 10 NN base pairs discussed in Chapter 1, AA (=TT) base steps takes on a particular significance because of its prominent role in the structure of A-tracts in solution and in A-tract-induced axis bending. Molecular dynamics results have shown that DNA bending and flexibility are highly correlated, i.e. steps that show the most intrinsic deformation from B-form DNA are also the most deformable[37]. The trend for the flexibilities for base steps involving A and T is predicted to be in the following order, starting from the most flexible: TA > AT >AA[37]. The difference in the flexibilities is consistent with the results of gel electrophoretic mobility studies, where A_4T_4 showed a large gel migration anomaly indicative of DNA bending, whereas T_4A_4 shows normal B-DNA gel migration behavior[125]. In our work, d(TAAAAAAAAAAT) (PAM 10) has the largest absolute $(\Delta\varepsilon)_{260}$ value, whereas d(TTAAAAAAAATT) (PAM 8) has the lowest absolute value of $(\Delta\varepsilon)_{260}$, although they both contain identical number of NN base pairs, i.e. 9 AA/TT, 1 AT, and 1 TA. The reason for the two extreme values now depends on the evaluation of the sequence context at both the 5'- and 3'- end. Since PAM 10 has AT base steps and PAM 8 has TT base steps, it is obvious that AT base steps stabilizes B*-form structure of A-tract better than TT base steps. This results in a more intense negative CD band at 260 nm for PAM 10. Absolute values of $(\Delta\varepsilon)_{260}$ for PAM

sequences of n = 3, 4, and 6 range between that of PAM 8 and PAM 10 since these sequences have less than 9 AA/TT base pairs, and more than one each of AT and TA base pairs .

PAE sequences show less difference in $(\Delta\varepsilon)_{260}$ values compared to PAM sequences, indicating that A-tract may have very little effect on the B*-form structure when it is located at the 3- end. Nevertheless, $(\Delta\varepsilon)_{260}$ values are useful for probing sequence effects. For example, PAM sequences of n = 3, 4, 6, and 8 have fewer AA/TT base steps compared to n = 10, and yet the difference between the largest and smallest $(\Delta\varepsilon)_{260}$ values for the PAE series is relatively less significant compared to the PAM series.

Although $(\Delta\varepsilon)_{260}$ does not directly relate to thermodynamic values, it plays a role in representing the balance between the sequence context within the A-tract and non-A-tract region. It should be noted that the ability to understand and predict stability depends on knowing the sequence context and structural information that the molecule will take based on the sequence.

3.7 Evaluation of the Nearest-Neighbor Model for A-Tract Oligomers

In Table 3.3, the comparison between experimental and predicted values shows that the NN model generally gives results consistent with the expected trend with respect to secondary structural determining sequences, i.e. there is a general relationship between length of A-tract and stability of an oligomer. For instance, the T_m increases from 39.3°C to 44.2°C for PAM sequences, and 38.1°C to 44.7°C for PAE sequences, going from the shortest to longest A-tract. However, there are very large differences between the thermodynamic parameters for identical nearest-neighbor interactions. Consider the

sequences d(TATTAAAATTAT) (PAM 4), d(TAATAAAATAAT) (PAM 4b), and d(TATAAAAAATAT) (PAM 6), all of which contain the same nearest-neighbor distributions, i.e. five AA/TT, three AT, and three TA base pair interactions. Experimentally determined values of T_m, ΔH°, and ΔS° for these three oligomers do not match their NN model predicted values. The average percentage error between the measured values and predicted values in T_m, ΔH°, and ΔS° are estimated to be approximately 5.0 %, 10.3 %, and 11.9 %, respectively. These differences reflect the complexity underlying DNA secondary structure, which can contribute to the stability of each of these sequences. The differences in structures of PAM 4, PAM 4b, and PAM 6, give rise to the differences in shapes of the CD difference spectra seen in Figure 3.16, and are likely the reason why all three of these sequences differ in terms of enthalpy and entropy. This evidence shows that the current NN model cannot estimate the thermodynamic values of A-tract oligonucleotides with the required degree of accuracy. These data are highly suggestive that improvement made to the current prediction model of A-tract oligonucleotides must not only consider the sequence context, but must also account for structural differences that a DNA molecule can adopt.

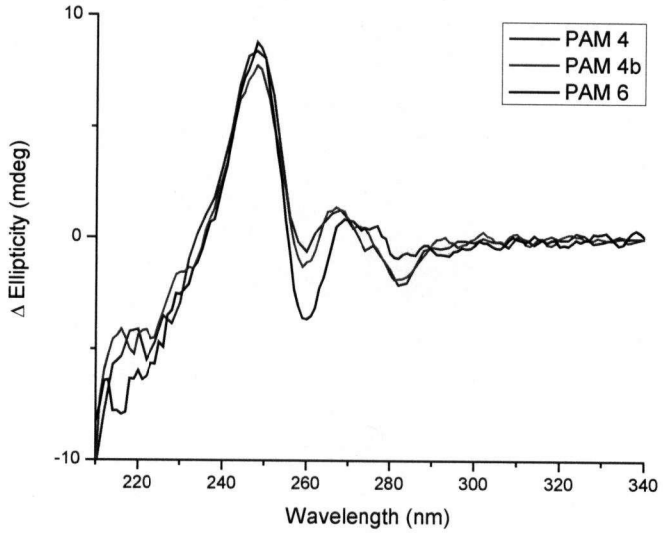

Figure 3.16: CD difference spectra of d(TATTAAAATTAT) (PAM 4), d(TAATAAAATAAT) (PAM 4b), and d(TATAAAAAATAT) (PAM 6), all of which contain the same nearest-neighbor distributions, i.e. five AA/TT, three AT, and three TA base pair interactions, and are thus predicted to have the same thermodynamic parameters. Structural differences in each of these sequences give rise to different enthalpy and entropy values based on experimental DSC results.

Chapter 4

The Impact of LNA on A-Tract Structure

The practical advantages of locked nucleic acids (LNA) have received considerable attention due to their therapeutic and diagnostic properties. In this chapter, a preliminary insight into the structural influence of LNA on the formation of B*-form characteristic of A-tracts will be examined. On the basis of our analysis, it is observed that the B*-form characteristics of poly(dA)·poly(dT) are attenuated in the presence of LNA.

4.1 Limitations of DNA Probes and Primers

The Human Genome Project and the need to elucidate the many molecular pathways that underlie all aspects of human health have motivated the development of many new oligonucleotide-based technologies for genome analyses, diagnostics, or therapeutics. For example, antisense nucleic acids have been used for silencing the expression of specific genes[136, 137] and DNA microarrays provide a way to measure gene expression[138]. Ideal oligonucleotide probes and primers will be able to discriminate between its intended target and all other targets under a given hybridization condition with minimal variation[139]. This would involve the ability to identify an optimal set of conditions for hybridization and to accurately predict the interaction with their respective targets of probes and primers of any length, any sequence, and any chemical composition. However, in practice, DNA-based technologies have not reached their full potential due to the challenges faced in the process of optimal probe and primer design. For example, during performance testing of probes and primers, it is difficult to measure the

accumulation of the oligonucleotide in the target site and uncertainties in delivery may lead to toxic effects. Low-probe hybridization efficiency due to specificity and biostability problems[140] caused by changes in secondary structure of the target sequence can also limit the potential of DNA probes and primers. These issues, as well as the increasing demand for potential antisense agents and diagnostic probes which have high selectivity and high-affinity recognition of complementary nucleic acid sequences has motivated an intensive search for nucleic acid analogues that have better properties than natural DNA-based oligonucleotides.

4.2 Nucleic Acid Analogues

Some DNA and RNA analogs exhibit improved stability and specificity compared to natural DNA and RNA, and they are becoming more commonly used for probes and primers and for antisense therapeutics[141, 142]. Several such chemically modified oligonucleotides have been developed and some are commercially available. It is beyond the scope of this chapter to present a thorough review, but the main types will be briefly described in order to provide a context for the locked nucleic acids (LNA), which is the type of primary interest in this work.

4.2.1 Peptide Nucleic Acids

Peptide nucleic acids (PNA) have the same base structure as DNA or RNA, but the sugar phosphate backbone consists instead of repeating N-(2-aminoethyl)-glycine units and the nucleobases are attached with methylenecarbonyl linkers[143]. The neutral character of the backbone of PNA eliminates the Coulombic repulsion that occurs in natural nucleic acid hybridization. Therefore, PNA binds with higher affinity to DNA and

readily forms PNA/DNA hybrid duplexes[144]. PNA has also been found to be stable against nuclease, protease, and peptidase activity, indicating that it is more robust in cells than DNA, RNA, and proteins. Together, these key features are the reasons why PNA is sometimes used in biosensors and as molecular recognition probes used in hybridization experiments[145]. However, the potential applications of PNA are limited due to its poor water solubility, synthesis complexity and expense, and tendency to form tertiary and quaternary structures in solution.

4.2.2 Phosphorothioate Oligonucleotides

Phosphorothioate oligonucleotides are chemically modified DNA or RNA oligonucleotides where a phosphate-oxygen bond is replaced by a phosphate-sulfur bond in the nucleic acid backbone[146]. The advantage of phosphorothioate oligonucleotides is that, like PNA oligonucleotides, they are more resistant to nuclease degradation[146] than DNA or RNA. Therefore, phosphorotioate oligonucleotides are extremely useful as antisense molecules inhibiting gene expression. An example of the first phosphorothioate oligonucleotide drug, Vitravene, has been used for the treatment of cytomegalovirus (CMV) retinitis in AIDS patients[147]. However, they bind poorly to target cells, exhibit lower hybridization affinity than PNA, and appear to show sequence non-specific toxicity in some systems[146].

4.2.3 Locked Nucleic Acids

Locked nucleic acids (LNA) is a novel class of conformationally restricted RNA nucleotide analogue in which the ribose ring is modified by an additional methylene linkage between the 2'-oxygen and the 4'-carbon[148, 149] (Figure 4.1). The methylene linkage 'locks' the sugar moiety into a C3'-endo conformation, resulting in the high affinity hybridization of LNA nucleotides to complementary DNA and RNA strands. Generally, synthetic LNA nucleotides can be inserted into any position within a DNA or RNA oligonucleotide by standard phosphoramidite chemistry using commercial DNA synthesizers[148, 149]. Since the synthesis and physical properties, such as solubility[150], of LNA closely resemble those for DNA, existing protocols for creating arrays need only minimal modifications[151].

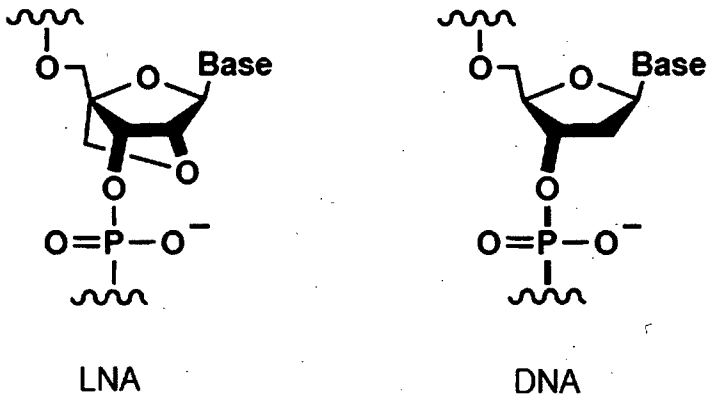

Figure 4.1: The molecular structures of a locked nucleic acid (LNA) nucleotide and a DNA nucleotide. The comparison between the two molecular structures shows that the ribose ring in LNA contains a 2'-O, 4'-C methylene linkage.

4.2.3.1 Chemical Properties of LNA

Besides its resistance to nuclease degradation[152], LNA contributes to the highest affinity ever obtained by Watson–Crick hydrogen bonding due to exceptionally high sequence specificity for the fully matched nucleic acid target[153, 154]. Oligonucleotides containing LNA exhibit enhanced thermal stabilities compared to unmodified DNA/DNA and DNA/RNA duplexes. The increased thermal stability is proposed to be the result of the bridging methylene group of LNA that confers conformational rigidity and the local organization of the phosphate backbone, leading to improved base stacking interactions[155]. LNA-incorporated duplexes have shown melting temperature increases relative to non-LNA duplexes of between 4°C to 10°C per LNA monomer[79, 148, 155], depending on the oligomers' length, sequence, and number of LNA bases in the oligomers.

4.2.3.2 Applications of LNA

The high affinity of hybridization demonstrated by pure LNA oligomers may allow substantial improvement of DNA microarray technology. In addition, LNA has been widely used in probe molecules in hybridization-based diagnostics such as SNP genotyping[156]. LNA is also recommended for use in any hybridization assay that requires high specificity and/or reproducibility e.g. dual labeled probes, *in situ* hybridization probes, molecular beacons and PCR primers[157]. Since LNA offers the possibility to adjust T_m values or primers and probes in multiplex assays, it provides a new means of primer and probe design that can overcome many of the design limitations associated with DNA oligonucleotides. Particular benefits of incorporating LNA into probes and primers include shorter lengths, increased selectivity, tight clamping of the 3'-end

irrespective of base composition, and the ability to hybridize at a specified temperature regardless of sequence[158].

4.3 Motivation

Detailed NMR studies have shown that fully modified LNA:DNA and LNA:RNA hybrids adopt a canonical A-type duplex morphology[159]. LNA modifications have been found to impact the overall conformation by changing the distribution of functional groups in the minor groove and the overall helical geometry relative to unmodified DNA[160], and by altering the counterion uptake and hydration pattern in the modified duplexes[140]. However, the structure and thermodynamics regarding the influence of LNA modification, particularly in A-tract containing oligonucleotides, is not very well known. Nevertheless, by keeping in mind that A-tracts play a role in replication and in transcriptional regulatory regions, the ability to control the properties of A-tracts through the use of LNA modifications may add to the potential of LNA as theurapeutic agents in antisense and antigene strategies. Using UV absorbance and CD methods, the structural perturbation of B*-form associated with the incorporation of LNA-modified duplex will be examined. It is also of interest to characterize and understand the thermodynamics of LNA modification in A-tract containing oligonucleotides.

4.4 Effects of LNA Substitution on Thermodynamic Stability

Table 4.1: Thermodynamic parameters of two LNA:DNA duplexes and their corresponding unmodified DNA duplexes. These results are obtained by differential scanning calorimetry experiments for 75 μM samples, each of which is suspended in a buffer containing 1 M NaCl, 10 mM Na_2HPO_4, and 1 mM Na_2(EDTA) (pH 7.0). (Reproduced with permission from Curtis Hughesman)

Name	Sequence[a]	T_m (°C)	ΔH° (kcal/mol)	ΔS° (cal/mol·K)
EE07	d(AAAAAAAAAAAA)	47.7	74.9	211.9
ALNA1	d(AAA^L AAA^L AAA^L AAA)	52.3	71.4	197.7
EE08	d(TTTTATAATAAA)	36.2	65.0	188.5
ALNA2	d($TTT^LTAT^LAAT^LAAA$)	43.1	67.5	191.8

[a] Superscript L refers to LNA modifications.

The T_m prediction tool for DNA-LNA duplexes exist[159], but since it has been reported to have a relatively large standard deviation of 1.6°C and 5.0°C for DNA and DNA–LNA mixmer oligonucleotides[80], respectively. Hence, the predicted values are not listed in the way that has been done for sequences listed in Table 3.3. The higher prediction error for LNA oligonucleotides may be attributed to their more complex chemical properties.

Based on the thermodynamic results in Table 4.1, the comparison between T_m of ALNA1 and ALNA 2 with their respective natural analogs, EE07 and EE08, reveals that the incorporation of three locked bases in ALNA1 and ALNA2 leads to a considerable increase in T_m, indicating that the LNA modified duplexes are much more stable than their corresponding unmodified duplexes. The increased thermal stability resulting from the incorporation of LNA monomers can be analyzed through the values for the change in ΔH° (ΔΔH°) and change in ΔS° (ΔΔS°), respectively, based on equations (4.1) and (4.2)[79]:

$$\Delta\Delta H^\circ = \Delta H^\circ_{LNA+DNA:DNA} - \Delta H^\circ_{DNA:DNA} \quad (4.1)$$

and

$$\Delta\Delta S^\circ = \Delta S^\circ_{LNA+DNA:DNA} - \Delta S^\circ_{DNA:DNA} \quad (4.2)$$

where the subscript LNA+DNA:DNA refers to the duplex incorporated with LNA monomers and DNA:DNA refers to the control DNA duplex. A negative $\Delta\Delta H^\circ$ indicates a favorable enthalpy change, whereas a negative $\Delta\Delta S^\circ$ represents an unfavorable entropy loss[140]. Therefore, the enhanced thermal stability in ALNA1 can be attributed to its more enthalpically favorable configuration, as implicated by the decrease in the enthalpic contribution ($\Delta\Delta H^\circ = -3.5$ kcal/mol). This decrease is accompanied by a smaller entropy value relative to the unmodified DNA duplex ($\Delta\Delta S^\circ = -14.2$ cal/mol·K). The opposite is true for the entropically favored configuration of ALNA2, with $\Delta\Delta H^\circ = 2.5$ kcal/mol and $\Delta\Delta S^\circ = 3.3$ cal/mol·K. The enthalpically driven stability for ALNA1 and entropically driven stability for ALNA 2 is in agreement with the net result observed for other LNA:DNA duplexes[140].

The thermodynamic behavior exhibited by the two LNA:DNA duplexes relative to their corresponding DNA:DNA duplexes can be explained by the general phenomenon of enthalpy versus entropy compensation. The enthalpic term is mainly associated with hydrogen bonding energies and van der Waals interactions, whereas rearrangements of the molecules, solvent water, and counterions are manifested in the entropic term[140]. The formation of hydrogen bonds and base stacking interactions during the annealing process of DNA duplexes are enthalpically favored, but the loss of degree of freedom is entropically unfavorable and is manifested in a negative entropy value. The compensating nature observed in terms of enthalpy and entropy ensures that the changes

in overall binding free energy, $\Delta G°$, are small, permitting readily reversible associations in solution[161]. The thermodynamic results for ALNA1 and ALNA2 show the impact of LNA substitution to either enthalpy or entropy relative to the unmodified duplexes. For ALNA1 and ALNA2, the locked C3'-*endo* conformation of the locked adenine bases locally organizes the phosphate backbone in order to increase the stacking efficiency of the nucleobases which is enthalpically favored[155].

4.5 UV Absorbance and CD Analysis of LNA/DNA duplex

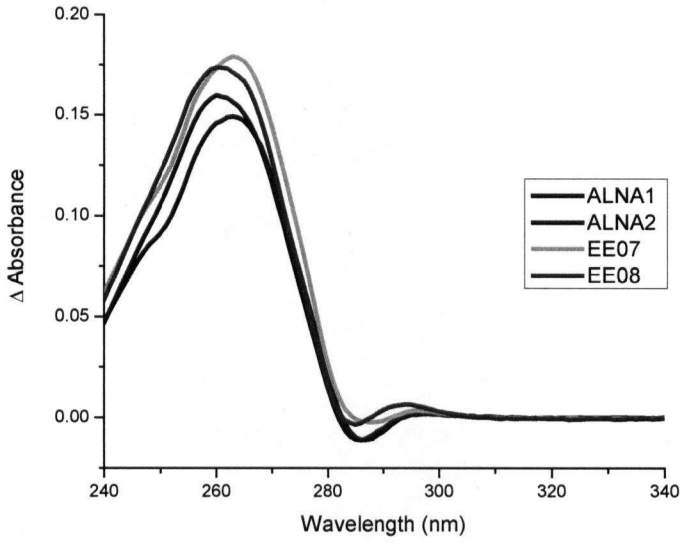

Figure 4.2: UV absorbance difference spectra of d(AAA^{L} AAA^{L} AAA^{L} AAA) (ALNA1) and d(TTT^{L}TAT^{L}AAT^{L}AAA) (ALNA2) obtained by subtracting the UV absorbance spectrum at 15°C from the spectrum at 75°C. Comparison is made with the UV absorbance difference spectra of the control sequences $d(A)_{12}$ (EE07) and d(TTTTATAATAAA) (EE08) to show the effect of the incorporation of LNA nucleotides.

Although ALNA1 and ALNA2 shows enhanced thermal stabilities, the UV absorbance difference spectra in Figure 4.2 displays lower peak maxima intensities for ALNA1 and ALNA2 compared to EE07 and EE08, respectively, indicating increased

hypochromicity due to the greater effect of base-stacking in ALNA1 and ALNA2. The general shapes of the difference spectra of ALNA1 and ALNA2 are very similar to that of their respective natural analogs, EE07 and EE08, indicating similar conformational characteristics.

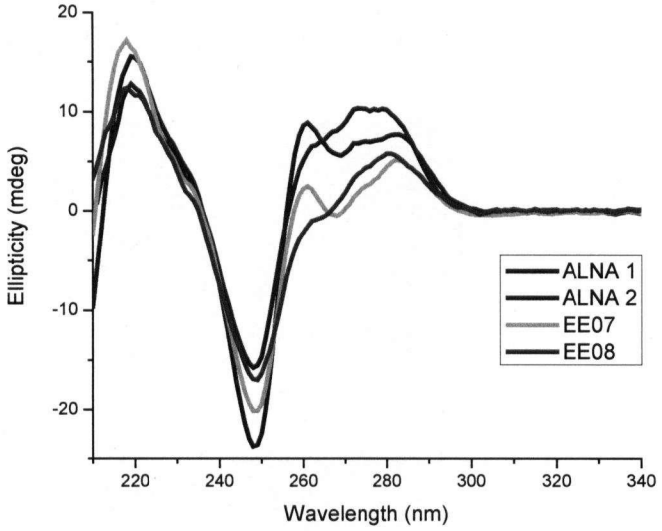

Figure 4.3: CD spectra at 15°C of d(AAA^{L} AAA^{L} AAA^{L} AAA) (ALNA1) and d(TTT^{L}TAT^{L}AAT^{L}AAA) (ALNA2) in comparison to their respective natural analogs, $d(A)_{12}$ (EE07) and d(TTTTATAATAAA) (EE08). The features of the peaks located between 260 – 300 nm for ALNA1 and ALNA2 are very similar to that of EE07 and EE08, respectively, but with relatively higher intensities in this region.

Figure 4.3 shows the CD spectrum of ALNA1 and ALNA2 compared to EE07 and EE08, respectively. The similarity in spectral shapes indicates that the modified duplexes share certain common characteristics with their corresponding unmodified duplexes in terms of base stacking geometries. However, in both cases, the spectra of the LNA modified duplexes exhibit a higher intensity for the bands located in the region of 260 – 300 nm. The ratio between the intensity of the 260 nm CD bands of ALNA1 and EE07 reveals an enhancement by a factor of 3.3, implying that the presence of the locked bases in ALNA1 and ALNA2 increases the conformational stability within the molecule.

Given that a duplex conforms to an A-form helix at the site of the locked base[140], it is expected that the structures of ALNA1 and ALNA 2 would exhibit spectral characteristics of A-form. This is in contrast to our findings since the CD spectra of ALNA1 seem to accentuate the conformation adopted by their respective unmodified sequences. The interpretation of this result is most likely that the CD shoulder at 260 nm indicates the presence of A-tracts rather than helix conformation. Also, the bands of enhanced intensities in those sequences containing LNA nucleotides indicates the fact that the sugar-phosphate rearranges in the vicinity of LNA nucleotides so as to further enhance base-stacking interactions.

4.6 Confirmation of the Presence of A-tracts

The incorporation of LNA monomers shows a marked increase in T_m, compared with the corresponding unmodified DNA duplexes, in accordance with the ability of LNAs to form the extremely stable Watson-Crick base-pairs[153]. The thermal stability for ALNA1 is due to an enthalpically favored conformational change in the presence of locked nucleotide bases, whereas the thermal stability for ALNA2 is entropically driven. Based on the analysis of our results, the B*-form characteristics of A-tracts are enhanced in the presence of LNA, although this observation requires further verification. Nevertheless, the presence of A-tracts is marked by the appearance of the shoulder at 260 nm in the CD spectra.

Chapter 5

Conclusion

5.1 General Summary

The B*-form structure induced by the presence of A-tracts can be characterized spectroscopically using UV absorbance and CD techniques. Although the analysis of UV difference spectra provides a rapid and simple method for qualitative structural information of DNA oligonucleotides, relying on a single optical technique may lead to incomplete characterizations and incorrect conclusions[162, 163]. Thus, CD measurements are carried out in addition to UV absorbance measurements to further evaluate the influence of A-tracts on the formation of B*- conformation, which may or may not be revealed using UV spectroscopy alone. For secondary structure determination, CD spectroscopy is particularly useful in detecting small changes in mutual orientation of neighboring bases in duplex DNA. Our UV absorbance and CD analysis suggest that the inherent tendency of forming B*-form by A-tract DNA oligomers can be affected, to different extent, by differences in A-tract length, the relative position of the A-tract position, presence of flanking sequences, and nearest-neighbor base pair interactions. The general objective of this structural study is to understand how each of these factors determine the extent of B*-form structure and how its formation is correlated with its thermodynamic properties.

5.2 B*-form Structure of A-tract Oligomers

In summary, the B*-form structure of A-tracts can be described as being rigid and less flexible than the standard B-form DNA. Its distinctive characteristics are slight base-pair inclination, high propeller twist, bifurcated hydrogen bonding, and a minor groove narrowing in the 5' to 3' direction. The most striking feature for the presence of B*-form is indicated by a 260 nm positive peak of the low temperature CD spectrum. Generally, the CD of A-tract containing oligonucleotides decreases with increasing temperature, suggesting a loss of secondary structure. Temperature variations perturb the A-tract DNA duplex structure, resulting in pronounced changes in their CD and UV absorbance spectra. One of the unique properties of A-tracts duplexes regards its spine of hydration in its minor groove, which has been proposed to provide an energetically favorable contribution that stabilizes the B*-form of the duplex structure[27]. Thus, the loss of secondary structure observed from our results may indicate a disruption of the spine of hydration, with a concomitant conformational alteration of the base pairs. The optical changes observed presumably arise from the latter event. The disruption of the spine of hydration consequently widens the minor groove geometry[113], based on the study of the nature by which daunomycin binds to the minor groove of poly(dA)·poly(dT). The binding interaction proceeds when daunomycin perturbs the structure of the polynucleotide in a manner similar to temperature.

A substantiated explanation for secondary structure loss is based on the junction model[47], in which deflection of the helix axis is localized at junctions between B*-form structure of A-tracts and B-form of non-A-tracts. At low temperature, a structural bend forms at the interphase between the A-tract and random sequence section because the

secondary structure of the A-tract is atypical. At high temperature, the secondary structure of an A-tract segment becomes similar to that of random sequence DNA, the junction disappears and the helix straightens[46].

5.3 Factors Governing the Propensity for B*-form

5.3.1 Effect of A-tract Length

The extent of B*-DNA conformation can be variable depending on the length of A-tracts. The change in UV absorbance at 260 nm is indicative of base-stacking interactions, resulting in increased magnitude in the 260 nm peak intensities of TDS when A-tract length increases.

The CD spectra also show an increase in both peak height and the increase in trough depth, also indicating base-stacking interactions become more pronounced as the length of the A-tract increases. Dependence of CD spectra on A-tract length manifested in the 248 nm peak intensity of the CD difference spectra. In our experiments, the enhanced 248 nm peak intensity is a result of the increase in the B*-form character in oligomers with longer A-tracts. Base-stacking interactions stabilizing the B*-form is embedded in the shape and intensity of a peak at 260 nm in the original CD spectra, i.e. oligomers with longer A-tracts ($n > 6$) adopt geometries closer to B*-form as a consequence of increased base-stacking interactions. Structural characteristics of A-tracts are conferred by the stacking of adenine bases so as to maximize π overlap, high propeller twist, and localization of cations within the minor groove[24]. Another particularly important aspect of B*-form may be the existence of an intrahelical cross-strand bifurcated hydrogen bond[164]. Favorable π overlap of adenine-adenine stacking affects the A-tract region, causing high propeller twist along the longitudinal axis, which

in turn is responsible for the formation of additional non-Watson-Crick hydrogen bonds across the major groove[133, 164, 165] and for the stabilization of the spine of hydration[166]. The bifurcated hydrogen bonds are formed when the N6 atom of adenine comes into close proximity with the O4 atom of thymine[164]. The existence of bifurcated hydrogen bonds implies that at least three adenines in tandem are needed to stabilize the bifurcated hydrogen bond interaction[164], but interestingly, at least four consecutive adenines are required to show the anomalously slow gel electrophoretic mobility of A-tracts. There is no clear evidence for the extent of each of these factors that comes into effect in an A-tract group of sequences, but it is believed that together, they contribute to the stabilization of B*-form[166].

In general, there is a reasonably good quantitative agreement between trends observed for TDS peak intensities at 260 nm (Figure 3.3) and results from CD difference peak intensities at 248 nm (Figure 3.10).

5.3.2 Positional Effects of A-tract

The relative positioning of A-tract has been observed to affect the amount of B*-form structure that is formed. When A-tract is adjacent to the 3'-end of non-A-tract regions (PAE series), the extent of changes in the CD spectra is minimal. The CD spectral feature of the PAE series of sequences appears to resemble that of a reference B-form DNA structure, even in sequences with longer A-tracts. For the PAE series, the overall effect on the formation of B*-form is minimal or suppressed and the non-A-tract region becomes dominant in determining the overall DNA conformation. When A-tract is located between two non-A-tract regions (PAM series), there exists a more pronounced propensity for B*-form with increasing A-tract length.

The positional effects of A-tracts based on the comparison between PAE and PAM sequences validates previous hypothesis that B*-form builds up progressively from the 5'-end[128], mainly because A-tracts displays a unique and nonuniform structure[167].

5.3.3 Sequence Context of Flanking Sequences

Sequences containing the same central A-tract flanked symmetrically on both sides by AT and TA base pairs in different order, d(TATTAAAATTAT) (PAM4), d(TAATAAAATAAT) (PAM4b), and d(ATATAAAATATA) (PAM4c), display differences in the CD difference spectra, particularly in the region of 260 – 280 nm. This implies the differential effect of flanking sequences on the overall formation of B*-form. A unique feature associated with A-tract DNA is that a 5′-AT-3′ step does not disrupt the narrowing of the minor groove width of an A-tract and other properties associated with the A-tract[27]. Since the 5′-end of an A-tract is wider than the 3′-end, the width of the minor groove at the 5′- AT step may allow for a more optimally stacked interaction within the A-tract region, as evidenced by a more enhanced negative band at 260 nm in the CD difference spectrum of d(ATATAAAATATA) (PAM 4c). In contrast, a 5′-TA-3′ step is disruptive to an A-tract and thus, CD conformational changes approaches that of a canonical B-form DNA structure.

Qualitative comparison based on our results have shown that flanking sequences can modulate the extent of formation of B*-form. The results presented here suggest that the propensity for B*-form formation is increased in the following flanking sequence context: TA < TT < AT. Such influence is possibly due to the interactions between A-tracts and flanking (non-A-tract) regions because A-tracts are not polymorphic in nature

and their effect extends into the flanking sequences neighboring it on its 3′-side[167]. Our results have shown that the effect of the flanking sequence is structural in nature and can be explained by the nonuniformity of the A-tract structure.

5.3.4 Nearest-Neighbor Base Pair Interactions

DSC studies by Curtis Hughesman of the Haynes laboratory have demonstrated that the thermodynamic parameters of A-tract oligonucleotides, especially those with identical nearest-neighbor pairs, are not well predicted by the most current nearest-neighbor model. This is clear evidence for the complexity of DNA structure, which may be overlooked by simple nearest-neighbor analysis.

The comparison of CD difference spectra for sequences which have the same nearest-neighbor interactions have shown that stability prediction must be based on the type of structure will take, besides simply knowing the sequence of oligonucleotides containing A-tracts. Specifically, a new and improved model must consider the properties of A-tract oligonucleotides, which have been the underlying factor for the differences in thermal stability.

5.3.5 Conformational Effects

In addition to the increasing the thermal stability, our structural data shows that the presence of LNA provides the possibility of controlling the effects of stacking in the B*-form structure of A-tracts. This implies that the constrained conformation induced by the additional methylene linkage in LNA further contributes to the rigidity of the A-tract structure, and helps to strengthen the stacking interactions of the adenine residues within the A-tract. Hence, the enthalpically-driven stabilization due to LNA compensates for

the loss in entropy due to decreased degrees of freedom in the well-stacked structure. It is, however, difficult to draw any final conclusions on this factor involving LNA because LNA is known to stabilize the duplex in an A-form conformation. The next obvious step is to determine the spectral characteristics that distinguishes B*-form from A-form and to carry more experiments comparing both LNA hybrid duplexes and their corresponding unmodified DNA duplexes. It is important to note that our results-to-date relating to the conformational effects on A-tract structure using LNA bases confirms that the characteristic shoulder at 260 nm of the CD spectrum indicates the presence of A-tract.

5.4 Impact of A-tract Structure on its Thermodynamic Properties

Although the available quantitative data on B*-form is limited, we have shown that the unique structure attributed to the presence of A-tracts is generally responsible for the increased thermal and thermodynamic stabilization. The stability of A-tract containing DNA oligomers has been ascribed to the extent of B*-form structure, which has been explained in terms of A-tract length, position, flanking sequences, number of nearest-neighbor interactions, and the presence of locked nucleotide bases. This stresses the significance of the overall B*-form structure. The B*-form structure is stabilized by the compact base stacking interactions of several adenine bases in longer A-tracts. Efficient base stacking relates to better overlap of the π-electrons. In the thermodynamic sense, higher B*-form content results in increased thermal stabilization, which is governed by enthalpy-entropy effects, because more energy is required to destroy the highly efficient base-stacking arrangement in A-tracts.

5.5 Future Directions

Our current results have opened new directions for an outlook on both fundamental and practical concerns. Undoubtedly, the current database of A-tract sequences must first be expanded and tested experimentally in order to further evaluate and improve the reliability of spectroscopic methods for secondary structure determination. At this stage, attention is focused on AT-rich sequences containing A-tracts. This list of sequences will be expanded to accommodate other nearest-neighbor effects, involving for instance CG and GC base steps, to observe further influences of sequence context on B*-form conformation. Accumulation of these systematic studies would provide a more solid framework for rapid predictions for most, if not all, mixed sequences based on comparative sequence analysis.

It has also been shown that structural features will allow the refinement of thermodynamic parameters that can account for those characteristics. Further testing of a larger set of A-tract sequences will also serve to test the quality of new thermodynamic rules and additional secondary structure prediction algorithms. At present, this work may provide a starting point for the appropriate modification and refinement of existing structural models for A-tract DNA oligomers.

Base-stacking interactions in A-tracts is a dominant factor in the stabilization of B*-form. Hydrogen bonds, electrostatic interactions of the charged phosphate groups, and thermodynamic effects (entropy of internal motions and solvent molecules) also contribute to helix stability. Since the stability of A-tract containing DNA duplexes is a sum of all these factors, another interesting avenue to consider is the quantification of the relative contributions from each of these interactions to the total stability of B*-

conformation. This is an ambitious and somewhat difficult task that has not been approached because of the non-linear additive effects of many different stabilization factors[164].

The B to A transition, known to regulate protein-DNA recognition, has been studied in detail through mixed ethanol water solvent experiments and molecular dynamics (MD) simulations[168]. The B to A transition is not a spontaneous process because a significant activation barrier exists between the two helical states, whereas the A to B transition occurs spontaneously on the nanosecond time scale. In a similar fashion, well-characterized structural studies on B* versus B-conformation will provide a basis for more detailed MD simulations on the B* ↔ B helix transition. Since we know the optimal range of chain lengths that drives the different extent of formation of B*-form in A-tracts, it is possible to analyze the B* ↔ B equilibrium owing to large changes of the CD and of the UV absorbance spectra[168]. The dynamics of the B* ↔ B-DNA transition will be extremely valuable to further understand how this transition is mediated by A-tracts. For instance, what are the intermediates that exist, if any, for this particular transition? If so, can their existence affect the preference of formation of one conformation over the other? Can dynamics be responsible for some characteristics of the current experimental observations?

The role of DNA thermodynamics in molecular biology applications is well-documented and has been emphasized in the introductory chapter of this thesis. A brief overview on the rules and regulations for probe and primer design was mentioned, but was not listed in details because it is not the focus our work. However, many aspects of

the findings in this work do overlap the goals of perfecting those guidelines for practical applications, such as consideration of template secondary structure. The presence or formation of secondary structure by target or probe DNA is known to inhibit probe/primer hybridization, leading to poor or no yield of the product. The formation of unfavorable secondary structures of a primer can reduce the binding of primers to the template, depending on factors such as temperature and base compositions. This decreases the availability of primers to the reaction and adversely affects the product yield of PCR amplification. Hence, if an unwanted type of secondary structure is known and predicted to form, careful measures can be taken to avoid them in order to optimally take advantage of the time and effort put into those applications.

References

1. Watson, J. D. and Crick, F. H. C. Molecular structure of nucleic acids. *Nature* **171**, 737-738 (1953).
2. Watson, J. D. and Crick, F. H. C. Genetical implications of the structure of deoxyribonucleic acid. *Nature* **171**, 964-967 (1953).
3. Saenger, W. *Principles of Nucleic Acid Structure* (Springer, New York, 1984).
4. Voet, D., Voet, J. G., and Pratt, C. V. *Fundamentals of Biochemistry.* (John Wiley and Sons, Inc., New York, 1999)
5. Marky, L. A. and Breslauer, K. J. Origins of netropsin binding affinity and specificity: correlations of thermodynamic and structural data. *Proceedings of the National Academy of Science USA* **84**, 4359-4363 (1987).
6. Vorlickova, M. Conformational transitions of alternating purine-pyrimidine DNAs in perchlorate ethanol solutions. *Biophysical Journal* **69**, 2033–2043 (1995).
7. Davies, D. R. and Baldwin, R. L. X-ray studies on two synthetic DNA copolymers. *Journal of Molecular Biology* **6**, 251 – 255 (1963).
8. Waring, M. Facilitating structural transitions in DNA. *Proceedings of the National Academy of Science USA* **97**, 11685 – 11687 (2000).
9. Maniatis, T., Venable, J. M., and Lerman, L.S. The structure of Ψ DNA. *Journal of Molecular Biology* **84**, 37 – 64 (1974).
10. Fuller, W., Wilkins, M. H. F., Wilson, H. R., and Hamilton, L. D. The molecular configuration of deoxyribonucleic acid. IV. X-ray diffraction study of the A-form. *Journal of Molecular Biology* **12**, 60 – 76 (1965).
11. Arnott, S., Fuller, W., Hodgson, A., and Prutton, I. Molecular conformations and structure transitions of RNA complementary helices and their possible biological significance. *Nature.* **220**, 561 – 564 (1968).
12. Arnott, S. The geometry of nucleic acids. *Progress in Biophysics and Molecular Biology* **21**, 265-319 (1970).
13. Wang, A. H. J., Quigley, G. J., Kolpak, F.J., Crawford, J. L., van Boom, J. H., Van der Marel, G., and Rich, A. Molecular structure of a left-handed double helical DNA fragment at atomic resolution. *Nature* **282**, 680-686 (1979).
14. Rao, S. N. and Kollman, P. On the Role of Uniform and Mixed Uniform Sugar Puckers in DNA Double Helical Structures. *Journal of the American Chemical Society* **107**, 1611-1617 (1985).
15. Dickerson, R. E. and Ng, H. L. DNA structure from A to B. *Proceedings of the National Academy of Science USA* **98**, 6986-6988 (2001).
16. Yoon, C., Prive, G. G., Goodsell, D. S. and Dickerson, R. E. Structure of an alternating B-DNA helix and its relationship to A-tract DNA. *Proceedings of the National Academy of Science USA* **85**, 6332-6336 (1988).
17. Dickerson, R. E. DNA structure from A to Z. *Methods in Enzymology* **211**, 67-127 (1992).
18. Hud, N. V. and Plavec, J. A unified model for the origin of DNA sequence-directed curvature. *Biopolymers* **69**, 144–159 (2003).

19. Tolstorukov, M. Y., Ivanov, V. I., Malenkov, G. G., Jernigan, R. L., and Zhurkin, V. B. Sequence-dependent B ↔ A transition in DNA evaluated with dimeric and trimeric scales. *Biophysical Journal* **81**, 3409–3421 (2001).
20. Wang, A. H. J., Quigley, G. J., Kolpak, F. J., Crawford, J. L., van Boom, J. H., van der Marel, G., and Rich, A. Molecular structure of a left handed double helical DNA fragment at atomic resolution. *Nature* **282**, 680-686 (1979).
21. Callahan L., Han F. S., Watt, W., Duchamp, D., Kezdy, F. J., and Agarwal, K. B- to Z-DNA transition probed by oligonucleotides containing methylphosphonates. *Biochemistry* **83**, 1617-1621 (1986).
22. Peck, L. J. and Wang, J. C. Energetics of B-to-Z transition in DNA. *Proceedings of the National Academy of Sciences USA* **80**, 6206-6210 (1983).
23. Arnott, S. and Selsing, E. Structures for the polynucleotide complexes poly(dA)·poly(dT) and poly(dT)·poly(dA)·poly(dT). *Journal of Molecular Biology* **88**, 509-521 (1974).
24. Nelson, H. C. M., Finch, J. T., Luisi, B. F., and Klug, A. The structure of an oligo(dA)·oligo(dT) tract and its biological implications. *Nature* **330**, 221-226 (1987).
25. Arnott, S., Chandrasekaran, R., Hukins, D. W. L., Smith, P. J. C., and Watts, L. Structural details of a double helix observed for DNAs containing alternating purine and pyrimidine sequences. *Journal of Molecular Biology* **88**, 523-533 (1974).
26. Bolshoy, A., McNamara, P., Harrington, R. E., and Trifonov, E. N. Curved DNA without A-A: Experimental estimation of all 16 DNA wedge angles. *Proceedings of the National Academy of Science USA* **88**, 2312-2316 (1991).
27. Chuprina, V. P. Anomalous structure and properties of poly (dA)·poly(dT). Computer simulation of the polynucleotide structure with the spine of hydration in the minor groove. *Nucleic Acids Research* **15**, 293-311 (1987).
28. Dickerson, R. E., and Drew, H. R. Structure of a B-DNA dodecamer. II. Influence of base sequence on helix structure. *Journal of Molecular Biology* **149**, 761-786 (1981).
29. Lesser, D. R., Kurpiewski, M. R., Waters, T., Connolly, B. A., and Jen-Jacobson, L. Facilitated distortion of the DNA site enhances EcoRI endonuclease-DNA recognition. *Proceedings of the National Academy of Science USA* **90**, 7548-7552 (1993).
30. Burkhoff, A. M. and Tullius, T. D. The unusual conformation adopted by the adenine tracts in kinetoplast DNA. *Cell* **48**, 935–943 (1987).
31. MacDonald, D., Herbert, K., Zhang, X., Pologruto, T., Lu, P. Solution structure of an A-tract DNA bend. *Journal of Molecular Biology* **306**, 1081–1098 (2001).
32. Nadeau, J. G. and Crothers, D. M. Structural basis for DNA bending. *Proceedings of the National Academy of Science USA* **86**, 2622–2626 (1989).
33. Strahs, D. and Schlick, T. A-Tract bending: Insights into experimental structures by computational models. *Journal of Molecular Biology* **301**, 643–663 (2000).
34. Drak, J. and Crothers, D. M. Helical repeat and chirality effects on DNA gel electrophoretic mobility. *Proceedings of the National Academy of Science USA* **88**, 3074-3078 (1991).

35. Stellwagen, E., Lu, Y., and Stellwagen, N. C. Curved DNA molecules migrate anomalously slowly in free solution. *Nucleic Acids Research* **33**, 4425-4432 (2005).
36. Madhumalar, A. and Bansal, M. Structural insights into the effect of hydration and ions on A-Tract DNA: A molecular dynamics study. *Biophysical Journal* **85**, 1805-1816 (2003).
37. McConnell, K. J. and Beveridge, D. L. Molecular dynamics simulations of B'-DNA: Sequence effects on A-tract-induced bending and flexibility. *Journal of Molecular Biology* **314**, 23-40 (2001).
38. Chen, Y.Z. and Prohofsky, E. W. The role of a minor groove spine of hydration in stabilizing poly(dA)·poly(dT) against fuctuational interbase H-bond disruption in the premelting temperature regime. *Nucleic Acids Research* **20**, 415-419 (1992).
39. Hagerman, P. J. Sequence directed curvature of DNA. *Annual Reviews of Biochemistry* **59**, 755-781 (1990).
40. Ulanovsky, L. E. and Trifonov, E. N. Estimation of wedge components in curved DNA. *Nature* **326**, 720-722 (1987).
41. Ganunis, R. M., Guo, H., and Tullius, T. D. Effect of the crystallizing agent 2-methyl-2, 4-pentanediol on the structure of adenine tract DNA in solution. *Biochemistry* **35**, 13729-13732 (1996).
42. Drak, J. and Crothers, D. M. Helical repeat and chirality effects on DNA gel electrophoretic mobility. *Proceedings of the National Academy of Science USA* **88**, 3074-3078 (1991).
43. Dlakic, M. and Harrington, R.E. The effects of sequence context on DNA curvature. *Proceedings of the National Academy of Science USA* **93**, 3847-3852 (1996).
44. Katahira, M., Sugeta, H., and Kyogoku,Y. A new model for the bending of DNAs containing the oligo(dA) tracts based on NMR observations. *Nucleic Acids Research* **18**, 613–618 (1990).
45. Nejedly, K., Sykorova, E., Diekmann, S., and Palecek, E. Analysis of a curved DNA constructed from alternating dA_n:dT_n-tracts in linear and supercoiled form by high resolution chemical probing. *Biophysical Chemistry* **73**, 205-216 (1998).
46. Koo, H. S., Wu, H. M., and Crothers, D. M. DNA bending at adenine-thymine tracts. *Nature* **320**, 501-506 (1986).
47. Haran, T. E., Kahn, J. A., and Crothers, D. M. Sequence elements responsible for DNA curvature. *Journal of Molecular Biology* **244**, 135-143 (1994).
48. Shatzky-Schwatz, M., Arbuckle, N., Eisenstein, M., Rabinovich, D., Bareket-Samish, A., Haran, T. E., Luisi, B. F., and Shakked, Z. X-ray and solution studies of DNA oligomers and implications for the structural basis of A-tract dependent curvature. *Journal of Molecular Biology* **267**, 595-623 (1997).
49. Wu, H. M. and Crothers, D. M. The locus of sequence-directed and protein-induced DNA bending. *Nature* **308**, 509-513 (1984).
50. Zinkel, S. S and Crothers, D. M. DNA bend direction by phase sensitive detection. *Nature* **328**, 178-181 (1987).

51. Trifonov, E. N. and Sussman, J. L. The pitch of chromatin DNA is reflected in its nucleotide sequence. *Proceedings of the National Academy of Science USA* **77**, 3816-3820 (1980).
52. Trifonov, E. N. Sequence-dependent deformational anisotropy of chromatin DNA. *Nucleic Acids Research* **8**, 4041-4053 (1980).
53. Struhl, K. Naturally occurring poly(dA-dT) sequences are upstream promoter elements for constitutive transcription in yeast. *Proceedings of the National Academy of Sciences USA* **82**, 8419-8432 (1985).
54. Roque, A., Orrego, M., Ponte, I., and Suau, P. The preferential binding of histone H1 to DNA scaffold-associated regions is determined by its C-terminal domain. *Nucleic Acids Research* **32**, 6111–6119 (2004).
55. Beloin, C., Jeusset, J., Re'vet B., Mirambeau, G., Le He'garatt, F., and Le Cam, E. Contribution of DNA conformation and topology in right-handed DNA wrapping by the *Bacillus subtilis* LrpC Protein. *The Journal of Biological Chemistry* **278**, 5333–5342 (2003).
56. Skoog, D. A., Holler, F. J., and Nieman, T. A. *Principles of instrumental analysis*. (Harcourt Brace and Company, Philadelphia, 1998).
57. Hammes, G. G. *Spectroscopy for the biological sciences*. (Wiley-Interscience, New Jersey, 2005).
58. Rich, A. and Kasha, M. The $n \rightarrow \pi^*$ transition in nucleic acids and polynucleotides. *Journal of the American Chemical Society* **82**, 6197-6199 (1960).
59. Haque, K. A., Pfeiffer, R. M., Beerman, M. B., Struewing, J. P., Chanock, S. J., and Bergen, A. W. Performance of high-throughput DNA quantification methods. *BMC Biotechnology* **3**, 20-29 (2003).
60. Yakovchuk, P., Protozanova, E., and Frank-Kamenetskii, M. D. Base-stacking and base-pairing contributions into thermal stability of the DNA double helix. *Nucleic Acids Research* **34**, 564-574 (2006).
61. Falk, M. The UV spectra of native and denatured DNA. *Journal of the American Chemical Society* **86**, 1226-1228 (1964).
62. Tinoco, I. Jr. Hypochromism in polynucleotides. *Journal of the American Chemical Society* **82**, 4785-4790 (1960).
63. von Ashen, N., Oellerich, M., Armstrong, V. W., and Schutz, E. Application of a thermodynamic nearest-neighbor model to estimate nucleic acid stability and optimize probe design: Prediction of melting points of multiple mutations of apolipoprotein B-3500 and Factor V with a hybridization probe genotyping assay on the LightCycler. *Clinical Chemistry* **45**, 2094–2101 (1999)
64. Ihtshamul, H., Chowdhry, B. Z., and Chaires, J. B. Singular value decomposition of 3-D DNA melting curves reveals complexity in the melting process. *European Biophysics Journal* **26**, 419-426 (1997).
65. Movileanu, L., Benevides, J. M., and Thomas, G. J. Determination of base and backbone contributions to the thermodynamics of premelting and melting transitions in B-DNA. *Nucleic Acids Research* **30**, 3767-3777 (2002).
66. Albergo, D. D., Marky, L.A., Breslauer, K. J., and Turner, D. H. Thermodynamics of $(dG\text{-}dC)_3$ double-helix formation in water and deuterium oxide. *Biochemistry* **20**, 1409-1413 (1981).

67. Johnson, W. C. Jr. Circular dichroism and its empirical application to biopolymers. *Methods of Biochemical Analysis* **31**, 62-125 (1985).
68. http://en.wikipedia.org/wiki/Circular_Dichroism
69. Service, R. F. DNA chips survey an entire genome. *Science* **281**, 1122 (1998).
70. Binder, H. and Preibisch, S. Specific and nonspecific hybridization of oligonucleotide probes on microarrays. *Biophysical Journal* **89**, 337-352 (2005).
71. Li, X., He, Z., and Zhou, J. Selection of optimal oligonucleotide probes for microarrays using multiple criteria, global alignment and parameter estimation. *Nucleic Acids Research* 33, 6114–6123 (2005).
72. Reymond, N., Charles, H., Duret, L., Calevro, F., Beslon, G., and Fayard, J-M. ROSO: optimizing oligonucleotide probes for microarrays. *Bioinformatics* **20** 271–273 (2004).
73. Lilley, D. M. J. and Dahlberg, J. E. DNA Structures Part A: Synthesis and Physical Analysis of DNA. *Methods in Enzymology* **211**, 533-567 (1992).
74. SantaLucia, J. Jr., Allawi, H. T., and Seneviratne, P. A. Improved nearest-neighbor parameters for predicting DNA duplex stability. *Biochemistry* **35**, 3555-3562 (1996).
75. Erlich, H. A. Gelfand, D., Sninsky, J. J. Recent advances in polymerase chain reaction. *Science* **252**, 1643-1651 (1991).
76. Steger, G. Thermal denaturation of double-stranded nucleic acids: prediction of temperatures critical for gradient gel electrophoresis and polymerase chain reaction. *Nucleic Acids Research* **22**, 2760-2768 (1994).
77. Chakrabarti, M. C. and Schwarz, F. P. Thermal stability of PNA/DNA and DNA/DNA duplexes by differential scanning calorimetry. *Nucleic Acids Research* **27**, 4801-4806 (1999).
78. Wittung, P., Nielsen, P. E., Buchardt, O., Egholm, M., and Norden, B. *Nature* **368**, 561– 563 (1994).
79. McTigue, P. M., Peterson, R. J., and Kahn J. D. Sequence-dependent thermodynamic parameters for locked nucleic acid (LNA)-DNA duplex formation. *Biochemistry* **43**, 5388 (2004).
80. Tolstrup, N., Nielsen, P. S., Kolberg, J. G., Frankel, A. M., Vissing, H., and Kauppinen, S. OligoDesign: optimal design of LNA (locked nucleic acid) oligonucleotide capture probes for gene expression profiling. *Nucleic Acids Research* **31**, 3758–3762 (2003).
81. Chou, L. S., Meadows, C., Wittwer, C. T., and Lyon, E. Unlabeled oligonucleotide probes modified with locked nucleic acids for improved mismatch discrimination in genotyping by melting analysis. *Biotechniques* **39**, 644-650 (2005).
82. Wahlestedt, C. et al. Potent and nontoxic antisense oligonucleotides containing locked nucleic acids. *Proceedings of the National Academy of Science USA* **97** 5633–5638 (2000).
83. Oerum, H. and Wengel, J. Locked nucleic acids: a promising molecular family for gene-function analysis and antisense drug development. *Current Opinion in Molecular Therapeutics* **3**, 239–243 (2001).
84. Atkins, P. *Physical Chemistry.* (Freeman, New York, 1998).

85. Wu, P., Nakano, S., and Sugimoto, N. Temperature dependence of thermodynamic properties for DNA/DNA and RNA/DNA duplex formation. *European Journal of Biochemistry* **269**, 2821-2830 (2002).
86. Marky, L. A. and Breslauer, K. J. Calculating thermodynamic data for transitions of any molecularity from equilibrium melting curves. *Biopolymers* **26**, 1601-1620 (1987).
87. Rouzina, I. and Bloomfield, V. A. Heat capacity effects on the melting of DNA. 1. General aspects. *Biophysical Journal* **77**, 3242-3251 (1999).
88. Rouzina, I. and Bloomfield, V. A. Heat capacity effects on the melting of DNA. 2. Analysis of nearest-neighbor base pair effects. *Biophysical Journal* **77**, 3252-3255 (1999).
89. Naghibi, H., Tamura, A., and Sturtevant, J. M. Significant discrepancies between van't Hoff and calorimetric enthalpies. *Proceedings of the National Academy of Sciences USA* **92**, 5597-5599 (1995).
90. Weber, G. van't Hoff Revisited: Enthalpy of association of protein subunits. *Journal of Physical Chemistry* **99**, 1052-1059 (1995).
91. Holbrook, J. A., Capp, M. W., Saecker, R. M., and Record, M. T. Jr. Enthalpy and heat capcity changes for formation of an oligomeric DNA duplex: interpretation in terms of coupled processes of formation and association of single-stranded helices. *Biochemistry* **38,** 8409-8422 (1999).
92. Liu, Y. and Sturtevant, J. M. Significant discrepancies between van't Hoff and calorimetric enthalpies. *Biophysical Chemistry* **64**, 121-126 (1997).
93. Wu, P. and Sugimoto, N. Transition characteristics and thermodynamic analysis of DNA duplex formation: a quantitative consideration for the extent of duplex association. *Nucleic Acids Research* **28**, 4762-4768 (2000).
94. Chaires, J. B. Possible origin of differences between van't Hoff and calorimetric enthalpy estimates. *Biophysical Chemistry* **64**, 15-23 (1997).
95. Horn, J. R., Russell, D., Lewis, E. A., and Murphy, K. P. van't Hoff and calorimetric enthalpies from isothermal titration calorimetry: are there significant discrepancies? *Biochemistry* **40**, 1774-1778 (2001).
96. Borer, P. N., Dengler, B., Tinoco, I. Jr., and Uhlenbeck, O. C. Stability of ribonucleic acid double-stranded helices. *Journal of Molecular Biology* **86**, 843-853 (1974).
97. Breslauer, K. J., Frank, R., Blocker, H., and Marky, L. A. Predicting DNA duplex stability from the base sequence. *Proceedings of the National Academy of Sciences USA* **83**, 3746-3750 (1986).
98. Wu, P., Nakano, S., and Sugimoto, N. Temperature dependence of thermodynamic properties for DNA/DNA and RNA/DNA duplex formation. *European Journal of Biochemistry* **269**, 2821-2830 (2002).
99. Santa Lucia, J. Jr. A unified view of polymer, dumbbell, and oligonucleotide DNA nearest-neighbor thermodynamics. *Proceedings of the National Academy of Sciences USA* **95**, 1460–1465 (1998).
100. Santa Lucia, J. Jr. and Hicks, D. The thermodynamics of DNA structural motifs. *Annual Review of Biophysics & Biomolecular Structure* **33**, 415–440 (2004).

101. Dlakic, M. and Harrington, R. E. The effects of sequence context on DNA curvature. *Proceedings of the National Academy of Sciences USA* **93**, 3847-3852 (1996).
102. Dlakic, M. and Harrington, R. E. Bending and torsional flexibility of G/C-rich sequences as determined by cyclization assays. *The Journal of Biological Chemistry* **270**, 29945-29952 (1995).
103. Goobes, R. and Minsky, A. Contextual equilibrium effects in DNA molecules. *Journal of Biological Chemistry* **276**, 16155–16160 (2001).
104. Doktycz, M. J., Morris, M. D., Dormady, S. J., Beattie, K. L., and Jacobson, K. B. Optical melting of 128 cctamer DNA duplexes: effects of base pair location and nearest neighbors on thermal stability. *Journal of Biological Chemistry* **270**, 8439-8445 (1995).
105. Paiva, A. M. and Sheardy, R. D. Influence of sequence context and length on the structure and stability of triplet repeat DNA oligomers. *Biochemistry* **43**, 14218-14227 (2004).
106. Peyret, N., Seneviratne, P. A., Allawi, H. T., and SantaLucia, J. Jr. Nearest-neighbor thermodynamics and NMR of DNA sequences with internal A·A, C·C, G·G, and T·T mismatches. *Biochemistry* **38**, 3468-3477 (1999).
107. Minetti, C. A. S. A., Remeta, D. P., Miller, H., Gelfand, C. A., Plum, G. E., Grollman, A. P., and Breslauer, K. J. The thermodynamics of template-directed DNA synthesis: base insertion and extension enthalpies. *Proceedings of the National Academy of Sciences USA* **100**, 14719–14724 (2003).
108. Sugimoto, N., Satoh, N., Yasuda, K., and Nakano, S. Stabilization factors affecting duplex formation of peptide nucleic acid with DNA. *Biochemistry* **40**, 8444-8451(2001).
109. Owczarzy, R., Vallone, P. M., Goldstein, R. F., and Benight, A. S. Studies of DNA dumbbells VII: Evaluation of the next-nearest-neighbor sequence-dependent interactions in Duplex DNA. *Biopolymers* **52**, 29–56 (1999).
110. Mergny, J-L, Li, J., Lacroix, L., Amrane, S., and Chaires, J.B. Thermal difference spectra: A specific signature for nucleic acid structures. *Nucleic Acids Research* **33**, e138 (2005).
111. Lankas, F., Cheatham, T. E., Spackova, N., Hobza, P., Langowski, J., and Sponer, J. Critical effect of the N2 amino group on structure, dynamics, and elasticity of DNA polypurine tracts. *Biophysical Journal* **82**, 2592–2609 (2002).
112. Fasman, G. D. *Circular Dichroism and the Conformational Analysis of Biomolecules* (Plenum Press, New York, 1996).
113. Herrera, J. E. and Chaires, J. B. A premelting conformational transition in poly(dA)·poly(dT) coupled to daunomycin binding. *Biochemistry* **28**, 1993-2000 (1989).
114. Greve, J., Maestre, M. F., and Levin, A. Circular dichroism of adenine and thymine containing synthetic polynucleotides. *Biopolymers* **16**, 1489-1504 (1977).
115. Arnott, S., Chandrasekaran, R., Hall, I. H., and Puigjaner, L. C. Heteronomous DNA. *Nucleic Acids Research* **11**, 4141-4155 (1983).

116. Alexeev, D. G., Lipanov, A. A., and Skuratovskii, I. Y. Poly(dA)·poly(dT) is a B-type double helix with a distinctively narrow minor groove. *Nature* **325**, 821-823 (1987).
117. Chan, S. S., Breslauer, K. J., Hogan, M. E., and Kessler, D. J. Physical studies of DNA premelting equilibria in duplexes with and without homo dA-dT tracts: Correlations with DNA bending. *Biochemistry* **29**, 6161-6171 (1990).
118. Marky, L. A. and Macgregor, R. B. Jr. Hydration of dA·dT polymers: role of H_2O in the thermodynamics of ethidium and propidium intercalation. *Biochemistry* **29**, 4805-4811 (1990).
119. Bhattacharyya, D., Kundu, S., Thakur, A. R., Majumdar, R. *Journal of Biomolecular and Structural Dynamics* **17**, 289-300 (1999).
120. Chan, S. S., Breslauer, K. J., Austin, R. H., Hogan, M. E. Thermodynamics and premelting conformational changes of phased $(dA)_5$ tracts. *Biochemistry* **32**, 11776-1 1784 (1993).
121. Jean, J. M. and Hall, K. B. Stacking-unstacking dynamics of oligodeoxynucleotide trimers. *Biochemistry* **43** 10277-10284 (2004).
122. Basham, B., Schroth, G. P., and Ho, P. S. An A-DNA triplet code: Thermodynamic rules for predicting A- and B-DNA. *Proceedings of the National Academy of Science USA* **92**, 6464-6468 (1995).
123. Scarlett, G. P., Elgar, S. J., Cary, P. D., Noble, A. M., Orford, R. L., Kneale, G. G., and Guille, M. J. Intact RNA-binding domains are necessary for structure-specific DNA binding and transcription control by CBTF during Xenopus development. *Journal of Biological Chemistry* **279**, 52447-52455 (2004).
124. Edmondson, S. P., and Johnson, W. C. Base tilt of poly (dA)·poly(dT) and poly (dAT)·poly(dAT) in solution determined by linear dichroism. *Biopolymers* **24**, 825-841 (1985).
125. Stefl, R., Wu, H., Ravindranathan, S., Sklena, V., and Feigon, J. DNA A-tract bending in three dimenstions: solving the dA_4T_4 vs. dT_4A_4 conundrum. *Proceedings of the National Academy of Sciences USA* **101**, 1177-1182 (2004).
126. Gudibande, S. R., Jayasena, S. D. and Behe, M. J. CD studies of double-stranded polydeoxynucleotides composed of repeating units of contiguous homopurine residues. *Biopolymers* **27**, 1905-1915 (1988).
127. Brahms, S. and Brahms, J. G. DNA with adenine tracts contains poly(dA)·poly(dT) conformational features in solution. *Nucleic Acids Research* **18**, 1559-1564 (1990).
128. Mollegaard, N. E., Bailly, C., Waring, M. J., and Nielsen, P. E. Effects of diaminopurine and inosine substitutions on A-tract induced DNA curvature. Importance of the 3'-A-tract junction. *Nucleic Acids Research* **25**, 3497-3502 (1997).
129. Kopka, M. L., Goodsell, D. S., Han, G. W., Chiu, T. K., Lown, J. W., and Dickerson, R. E. Defining GC-specificity in the minor groove: side-by-side binding of the di-imidazole lexitropsin to C-A-T-G-G-C-C-A-T-G. *Structure* **5**, 1033-1046 (1997).
130. White, S., Szewczyk, J. W., Turner, J. M., Baird, E. E., and Dervan, P. B. Recognition of the four Watson-Crick base pairs in the DNA minor groove by synthetic ligands. *Nature* **391**, 468-471 (1998).

131. Dixit, S. B., Pitici, F., and Beveridge, D. L. Structure and axis curvature in two $dA_6 \cdot dT_6$ DNA oligonucleotides: Comparison of molecular dynamics simulations with results from crystallography and NMR spectroscopy. *Biopolymers* **75**, 468-479 (2004).
132. Breslauer, K .J., Frank, R., Blocker, H., and Marky, L. A. Predicting DNA duplex stability from the base sequence. *Proceedings of the National Academy of Sciences USA* **83**, 3746-3750 (1986).
133. Digabriele, A. D., Sanderson, M. R., Steitz, T. A. Crystal lattice packing is important in determining the bend of a DNA dodecamer containing an adenine tract. *Proceedings of the National Academy of Sciences USA* **86**, 1816-1820 (1989).
134. Blake, R. D. and Delcourt, D. G. Thermal stability of DNA. *Nucleic Acids Research* **26**, 3323–3332 (1998).
135. Paiva, A. M. and Sheardy, R. D. Influence of sequence context and length on the structure and stability of triplet repeat DNA oligomers. *Biochemistry* **43**, 14218-14227 (2004).
136. Opalinska, J. B. and Gewirtz, A. M. Therapeutic potential of antisense nucleic acid molecules. *Science STKE* **206**, 1-5 (2003).
137. Crooke, S. T. Progress in antisense technology. *Annual Review of Medicine* **55**, 61-95 (2004).
138. Kane, M. D., Jatkoe, T. A., Stumpf, C. R., Lu, J., Thomas, J. D., and Madore, S. J. Assessment of the sensitivity and specificity of oligonucleotide (50mer) microarrays. *Nucleic Acids Research* **28**, 4552-4557 (2000).
139. Nielsen, H. B., Wernersson, R., and Knudsen, S. Design of oligonucleotides for microarrays and perspectives for design of multi-transcriptome arrays. *Nucleic Acids Research* **31**, 3491–3496 (2003).
140. Kaur, H., Arora, A., Wengel, J., and Maiti, S. Thermodynamic, counterion, and hydration effects for the incorporation of locked nucleic acid nucleotides into DNA duplexes. *Biochemistry* **45**, 7347-7355 (2006).
141. Nguyen, A., Zhao, C., Dorris, D., and Mazumder, A. Quantitative assessment of the use of modified nucleoside triphosphates in expression profiling: differential effects on signal intensities and impacts on expression ratios. *BMC Biotechnology* **2**, 4642-4648 (2002).
142. Matray, T., Gamsey, S., Pongracz, K., and Gryaznov, S. A remarkable stabilization of complexes formed by 2,6-diaminopurine oligonucleotide N3' → P5' phophoramidates. *Nucleosides Nucleotides Nucleic Acids* **19**,1553-1567 (2000).
143. Baker, E. S., Hong, J. W., Gaylord, B. S., Bazan, G. C., and Bowers, M. T. PNA/dsDNA Complexes: Site Specific Binding and dsDNA Biosensor Applications. *Journal of the American Chemical Society* **128**, 8484-8492 (2006).
144. Giesen, U., Kleider, W., Berding, C., Geiger, A., Orum, H., and Nielsen, P. E. A formula for thermal stability (T_m) prediction of PNA/DNA duplexes. *Nucleic Acids Research* **26**, 5004-5006 (1998).
145. Liu, J., Tiefenauer, L., Tian, S., Nielsen, P. E., and Knoll, W. PNA-DNA Hybridization Study Using Labeled Streptavidin by Voltammetry and Surface Plasmon Fluorescence Spectroscopy. *Analytical Chemistry* **78**, 470-476 (2006).

146. Gao, W. Y., Han, F. S., Storm, C., Egan, W., and Cheng, Y. C. Phosphorothioate oligonucleotides are inhibitors of human DNA polymerases and RNase H: implications for antisense technology. *Molecular Pharmacology* **41**, 223-229 (1992).
147. Lysik, M. A., Wu-Pong, S. Innovations in oligonucleotide drug delivery. *Journal of Pharmceutical Sciences* **92**, 1559-1573 (2003).
148. Koshkin, A. A., Singh, S. K., Nielsen, P., Rajwanshi, V. K., Kumar, R., Meldgaard, M., Olsen, C.E. and Wengel, J. LNA (Locked Nucleic Acids): Synthesis of the Adenine, Cytosine, Guanine, 5-Methylcytosine, Thymine and Uracil Bicyclonucleoside Monomers, Oligomerisation, and Unprecedented Nucleic Acid Recognition. *Tetrahedron* **54**, 3607-3630 (1998).
149. Wengel, J. Synthesis of 3'-*C*- and 4'-*C*-branched oligodeoxynucleotides and the development of locked nucleic acid (LNA). *Accounts of Chemical Research* **32**, 301-310 (1998).
150. www.sigmaldrich.com
151. Latorra, D., Campbell, K., Wolter, A., and Hurley, J. M. Enhanced allele-specific PCR discrimination in SNP genotyping using 30 locked nucleic acid (LNA) primers. *Human Mutation* **22**, 79-85 (2003).
152. Hertoghs, K. M. L., Ellis, J. H., and Catchpole, I. R. Use of locked nucleic acid oligonucleotides to add functionality to plasmid DNA. *Nucleic Acids Research* **31**, 5817-5830 (2003).
153. Koshkin, A. A., Nielsen, P., Meldgaard, M., Rajwanshi, V. K., Singh, S. K. and Wengel, J. LNA (locked nucleic acid): an RNA mimic forming exceedingly stable LNA:LNA duplexes. *Journal of the American Chemical Society* **120**, 13252-13260 (1998).
154. Silahtaroglu, A., Pfundheller, H., Koshkin, A., Tommerup, N., and Kauppinen, S. LNA-modified oligonucleotides are highly efficient as FISH probes. *Cytogenetic and Genome Research* **107**, 32-37 (2004).
155. Peterson, M., Nielsen, C. B., Nielsen, K. E., Jensen, G. A., Bondensgaard, K., Singh, S. K., Rajwanshi, V. K., Koshkin, A. A., Dahl, B. M. Wengel, J., and Jacobsen, J. P. The conformations of locked nucleic acids (LNA). *Journal of Molecular Recognition* **13**, 44-53 (2000).
156. Simeonov, A. and Nikiforav, T. T. Single nucleotide polymorphism genotyping using short, fluorescently labeled locked nucleic acid (LNA) probes and fluorescence polarization detection. *Nucleic Acids Research* **30**, e31, (2002).
157. Kvaerno, L. and Wengel, J. Investigation of restricted backbone conformations as an explanation for the exceptional thermal stabilities of duplexes involving LNA (Locked Nucleic Acid): synthesis and evaluation of abasic LNA. *Chemical Communications* **7**, 657-658 (1999).
158. Mouritzen, P., Nielsen, A. T., Pfundheller, H. M.; Choleva, Y., Kongsbak, L., and Moller, S. Single nucleotide polymorphism genotyping using locked nucleic acid (LNA). *Expert Review of Molecular Diagnostics* **3**, 27-38 (2003).
159. http://lna-tm.com
160. Marin, V., Hansen, H. F., Koch, T., Armitage, B. A. Effect of LNA modifications on small molecule binding to nucleic acids. *Journal of Biomolecular Structure and Dynamics* **21**, 841-850 (2004)

161. Searle, M. S. and Williams, D. H. On the stability of nucleic acid structures in solution: enthalpy-entropy compensations, internal rotations and reversibility. *Nucleic Acids Research* **21**, 2051 -2056 (1993).
162. Davis, T. M., McFail-Isom, L., Keane, E., and Williams, L. D. Melting of a DNA hairpin without hyperchromism. *Biochemistry* **37**, 6975-6978 (1998).
163. Sacca, B., Lacroix, L., and Mergny, J-L. The effect of chemical modifications on the thermal stability of different G-quadruplex-forming oligonucleotides. *Nucleic Acids Research* **33**, 1182-1192 (2005).
164. Digabriele, A. D. and Steitz, T. A. A DNA dodecamer containing an adenine tract crystallizes in a unique lattice and exhibits a new bond. *Journal of Molecular Biology* **231**, 1024-1039 (1993).
165. Coll, M., Frederick, C. A., Wang, A. H. J., and Rich, A. A bifurcated hydrogen-bonded conformation in the d(AT) base pairs of the DNA dodecamer d(CGCAAATTTGCG) and its complex with distamycin. *Proceedings of the National Academy of Science USA* **84**, 8385-8389 (1987).
166. Jose, D. and Porschke, D. Dynamics of the B-A transition of DNA double helices. *Nucleic Acids Research* **32**, 2251-2258 (2004).
167. Merling, A., Sagaydakova, N., and Haran, T. E. A-Tract polarity dominate the curvature in flanking sequences. *Biochemistry*, **42**, 4978 - 4984 (2003).
168. Ng, H. L., Kopka, M. L., and Dickerson, R. E. The structure of a stable intermediate in the A $\leftrightarrow$ B DNA helix transition. *Proceedings of the National Academy of Sciences USA* **97**, 2035-2039 (2000).

Appendix

1.0 Circular Dichroism Measurement Procedures

1.1 SYSTEM START-UP

1.1.1 Turn on the nitrogen supply. For measurements in the normal wavelength region (more than 190 nm), the proper flow rate of nitrogen gas is 3 litres/minute.
NOTE: Allow the nitrogen gas to purge the Xenon lamp compartment for about 10 minutes. The high intensity Xenon light source will convert oxygen to ozone, which destroys the optics.

1.1.2 Turn on the water recirculator. Check to ensure that the level of distilled water in the water recirculator is full.
NOTE: the level should be near the top of the reservoir – if it needs to be topped up use distilled water to avoid mineral deposits.

1.1.3 Open the sample compartment and confirm that there are no samples in the sample holder and that there are no obstructions to the light path.

1.1.4 Turn on the power to the computer, J-810 Spectropolarimeter, and the Peltier device.

1.1.5 Warm up the instrument for 30 minutes until it is stabilized after starting it.

1.1.6 Double click on the Spectra Manager Software icon on the desktop of the PC.

1.1.7 From the Spectra Manager window select the Spectrum Measurement application for scanning.

1.1.8 Checking of CD-value stability: Check often the CD-value stability with the sample while warming up the instrument. Pour an aqueous solution of 0.06% (w/v) ammonium d-10-camphorsulfonate into a 1 cm cell and set the cell in the instrument to make measurements with a wavelength of 290.5 nm for approximately 2 hours in the T-scan mode. If the stabilized CD value (value after base correction) remains within +190.4 mdeg (± 1%), it is normal.

1.2 SCANNING SET-UP

1.2.1 Ensure the scan parameters are set up as follows:

1.2.2 Select the Control Tab:

1.2.2.1 Bandwidth: set to 1 nm

1.2.2.2 Response: set to 4 seconds

1.2.2.3 Sensitivity: select Standard

1.2.2.4 Data Pitch: set to 1 nm

1.2.2.5 Scan Speed: set to 50 nm/min

1.2.2.6 Accumulations: set to 5

1.3 BASELINE CORRECTION

1.3.1 Click on the Measurement tab and select Baseline Correct.

1.3.2 Zero the spectropolarimeter with the same buffer used to prepare the test sample.

1.3.3 Click on the Start button to acquire the buffer spectrum.

1.3.4 Save the buffer spectrum to use as a baseline file.

1.4 MEASURING A SAMPLE

1.4.1 Load the correct baseline file.
1.4.2 Inspect the cuvette for particulates and ensure the cuvette is clean and free from scratches.
1.4.3 Place the sample in the sample holder.
1.4.4 Click on the Start button to acquire the spectrum of the sample and save the spectrum after acquisition.
1.4.5 Perform all readings within an assay using the same type of cuvette.

1.5 ZOOMING IN A SPECTRUM, AUTO SCALE and FULL SCREEN DISPLAY

1.5.1 To zoom in a spectrum using the mouse, click and drag the mouse so that a rectangle surrounds the area to be zoomed. The rectangle can be moved with keeping the same size. Once the rectangle is on the area to be zoomed, click the mouse again on the selected area.
1.5.2 To Autoscale the spectra move the cursor on the spectrum window and right click, select autoscale in the menu (changes the vertical axis to a proper size).
1.5.3 To return to full scale after zooming in, right click with the mouse on the spectrum window, select full from the menu.

1.6 SPECTRA OVERLAY

1.6.1 Select display (by right clicking on the file in the tree view window and select display) for all spectra to be overlaid. Select window and then join visible from the pull-down menu. To return each spectrum to an original window select split from the pull-down menu under window. To change the display style of overlaid spectra, select window and multi spectra from the pull down window, select a style from the submenu.

1.7 SYSTEM SHUT-DOWN

1.7.1 Confirm that all necessary CD data has been saved.
1.7.2 Close all the Spectra Manager Applications this will close down the connection to the J-810.
1.7.3 Remove all samples from the sample compartment.
1.7.4 Turn off the Water Recirculator power switch which is on the top left of the unit.
1.7.5 Turn off the Peltier temperature unit.
1.7.6 Turn off the J-810 the power switch.
1.7.7 Turn off the nitrogen supply.
1.7.8 Enter all activities in the instrument logbook.

2.0 UV Absorbance Measurement Procedures

2.1 SYSTEM START UP

2.1.1 Turn on the main power unit and allow the instrument to warm up for at least 30 minutes.
2.1.2 From the Start menu, click on Programs → Cary WinUV → Scan.
2.1.3 On the top toolbar options, click on the Setup tab.
  2.1.3.1 Under the X-Mode of the Cary tab, type in the start (340 nm) and end (200 nm) parameters of the wavelength region. Click OK.
  2.1.3.2 Under the Options tab, select Fixed SBW
  2.1.3.3 Under the Baseline tab, select Baseline Correction.
2.1.4 Use a Kimwipe to wipe down the sides of the cuvette and be careful to avoid touching the sides of the cuvette when putting it in the instrument.
2.1.5 Place the blank sample (buffer) in cell 1. Close the lid and click on the Start button.
2.1.6 The box in the upper left-hand corner will show that the instrument has been zeroed by displaying an absorbance of 0.000.
2.1.7 Remove the blank sample and place the oligomer sample into the same cell compartment. Ensure that the cuvette faces the same direction to ensure the same pathlength at all times.
2.1.8 Click Start to obtain a scan of the sample spectrum.

2.2 SAVING AND RETRIEVING DATA

2.2.1 To save data, go to "File" → "Save As". Enter a filename and click "Save" to save the file in the *.bsw format.
2.2.2 To open saved data, go to "File" → "Open". Select the desired file.

2.3 SYSTEM SHUT-DOWN

2.3.1 Save all data files and exit out of the program.
2.3.2 Turn off the main power unit.
2.3.3 Enter all activities in the instrument logbook.